Journal of Neuroinflammation

RESEARCH

Open Access

Transient CSF1R inhibition ameliorates behavioral deficits in *Cntnap2* knockout and valproic acid-exposed mouse models of autism

Jiao Meng[1,2], Pengming Pan[1,3], Gengshuo Guo[1,2], Anqi Chen[1,2], Xiangbao Meng[1,3*] and Heli Liu[1,2,4*]

Abstract

Microglial abnormality and heterogeneity are observed in autism spectrum disorder (ASD) patients and animal models of ASD. Microglial depletion by colony stimulating factor 1-receptor (CSF1R) inhibition has been proved to improve autism-like behaviors in maternal immune activation mouse offspring. However, it is unclear whether CSF1R inhibition has extensive effectiveness and pharmacological heterogeneity in treating autism models caused by genetic and environmental risk factors. Here, we report pharmacological functions and cellular mechanisms of PLX5622, a small-molecule CSF1R inhibitor, in treating *Cntnap2* knockout and valproic acid (VPA)-exposed autism model mice. For the *Cntnap2* knockout mice, PLX5622 can improve their social ability and reciprocal social behavior, slow down their hyperactivity in open field and repetitive grooming behavior, and enhance their nesting ability. For the VPA model mice, PLX5622 can enhance their social ability and social novelty, and alleviate their anxiety behavior, repetitive and stereotyped autism-like behaviors such as grooming and marble burying. At the cellular level, PLX5622 restores the morphology and/or number of microglia in the somatosensory cortex, striatum, and hippocampal CA1 regions of the two models. Specially, PLX5622 corrects neurophysiological abnormalities in the striatum of the *Cntnap2* knockout mice, and in the somatosensory cortex, striatum, and hippocampal CA1 regions of the VPA model mice. Incidentally, microglial dynamic changes in the VPA model mice are also reported. Our study demonstrates that microglial depletion and repopulation by transient CSF1R inhibition is effective, and however, has differential pharmacological functions and cellular mechanisms in rescuing behavioral deficits in the two autism models.

Keywords Autism, Microglia, CSF1R inhibitor, *Cntnap2* knockout mouse, Valproic acid-exposed mouse, Pharmacological heterogeneity

*Correspondence:
Xiangbao Meng
xbmeng@hsc.pku.edu.cn
Heli Liu
liuheli@hsc.pku.edu.cn
Full list of author information is available at the end of the article

Introduction

Autism spectrum disorder (ASD) is a range of heterogeneous neurodevelopmental disorders with core clinical symptoms manifested as impaired social interaction and communication, and restricted, repetitive and stereotypical patterns of behavior [1]. Hitherto, there are no drugs approved to treat the core symptoms of ASD [2]. The reason for this severe situation may lie in that the etiology of ASD presents high heterogeneity [3].

As etiological causes of ASD, both genetic and environmental risk factors may lead to immune dysregulation in autistic individuals and animal models [4]. Microglia, a key mediator of immune system and a sensor for pathological conditions in the CNS, can influence postnatal brain development, neuronal plasticity and circuit function [5–7]. Accumulating evidence suggests that microglial dysfunction has been linked to the occurrence of ASD. In people with ASD, augmented activation, abnormal morphology or increased density of microglia was observed in the cerebral cortex and subcortical areas, medial frontal gyrus, as well as the cerebellum [8–12]. Noteworthy, microglia in ~ 38% of postmortem cases with autism in one report by Morgan et al. [8] appeared markedly activated, and additional ~ 31% of cases presented marginally activated microglia. At the molecular level, transcriptional analysis and proteomic studies revealed that microglial activation-associated gene expression and complement molecules are upregulated in people with autism [13, 14]. Compared to typically developing individuals, a significant increase in primed microglia was seen by Lee et al. [15] in grey matter of ASD patients, while average cell number and volume of microglia did not differ in another case observed by Morgan et al. [16]. These studies suggest that a spectrum of microglial pathology in different patients reflects heterogeneity of ASD [15].

Microglial abnormality and heterogeneity are also seen in animal models of ASD. Prenatal valproic acid (VPA) exposure changed microglial phenotypes from resting to activated states in the prefrontal cortex and hippocampus regions of infant and adolescent VPA model rats, but microglial activation was alleviated in adulthood [17]. Microglia in VPA-induced autism model marmosets had abnormal morphology, and their processes were fragmented [18]. A positron emission tomography (PET) imaging showed an increased microglial activation in the prefrontal cortex and hippocampus in mature offspring of prenatal polyinosinic:polycytidylic acid (poly I:C) exposed rats [19], which are considered as an autism model induced by maternal immune activation (MIA) [20]. As a genetic model of ASD, *Fmr1* knockout (KO) mice displayed reduced microglia-mediated synaptic pruning in hippocampus [21]. BTBR mouse strain, an idiopathic ASD model, had a higher level of activated microglia [22]. Mouse offspring exposed to CASRP2-antibodies showed marked social interaction deficits and persistent microglial activation in the prefrontal and somatosensory cortices [23]. However, the number or morphology of microglia in *Cntnap2* (the gene encoding CASPR2) KO mice, in comparison with that in the wild type (WT) counterparts, was reported to have no difference [24].

Due to the emerging roles of microglia in brain development, plasticity and cognition [6], targeting microglia may act as a promising strategy for the treatment of neurological and psychiatric disorders including ASD [25, 26]. Predominantly expressed on microglia, colony stimulating factor 1-receptor (CSF1R) is necessary for microglia viability [27], and its expression is significantly upregulated in neurodegenerative diseases [28]. Inhibition of CSF1R signaling may lead to microglial depletion and repopulation that can have beneficial effects on behavior in different animal models of diseases, such as traumatic brain injury, Alzheimer's disease, Huntington's disease [28–37]. Ikezu et al. found that transient depletion of microglia caused by the CSF1R inhibitor PLX5622 can improve social impairment and stereotyped repetitive behavior in autism model mice with poly I:C-simulated maternal immune activation [38]. Interestingly, Elmore et al., who first discovered that CSF1R inhibitors can significantly deplete microglia, did not observe the effects of CSF1R inhibitors on social and other behaviors in healthy adult mice [27, 29]. For wild-type C57BL/6 mice, global depletion of microglia reversibly altered spatial memory, but resulted in no change in sociability behavior [39]. It seems that microglia are dynamic modulators in regulation of behavior effects [39, 40] due to their dynamic property [41]. However, it remains unknown how dynamic change of microglia occurs and whether such a dynamic change reversibly affects behaviors in autism model animals.

In this study, taking into account of etiological heterogeneity and microglial heterogeneity in ASD patients and animal models, we explored if CSF1R inhibition by PLX5622 could incur different pharmacological effects in treating *Cntnap2* KO and VPA-exposed autism model mice, which respectively represent genetic and environmental risk factors in etiology of autism [42, 43]. Meanwhile, we investigated dynamic shift of microglial population and morphology in VPA-exposed model mice treated with PLX5622. As a result, we found pharmacological effectiveness and heterogeneity of PLX5622 in treating the two models and mechanistic variance at the cellular level, and observed dynamic changes of microglia alongside behavioral improvement in the VPA model mice.

Methods

Generation of animals

Experimental mice were housed in individually ventilated cages (IVCs) with corncob bedding and maintained on a 12-h light–dark schedule with access to food and water ad libitum. Mice at age of 8 weeks were mated overnight, when the female mice were confirmed in estrus phase by microscopic examination of vaginal epithelial cells. The female mice were checked the next morning for the presence of a vaginal plug that marked the day as embryonic day 0.5 (E0.5). Pregnant female mice were transferred to a single cage and left undisturbed, except for necessary cage cleaning. The day of parturition was designated as postnatal day (P0). On postnatal day 21 (P21), offspring were housed separately according to sex, genotype and drug treatment, in groups of 3–5 mice per cage. Only male offspring were subjected to drug treatment and used for behavioral and cellular studies. Two male and two female *Cntnap2* heterozygous KO (*Cntnap2*$^{\pm}$, Jackson Laboratory (#017482)) mice at the C57BL/6 J background were a gift from Professor Jiada Li's lab in Central South University (Changsha, China). *Cntnap2* homozygous KO (*Cntnap2*$^{-/-}$) and WT and mice were obtained from heterozygous *Cntnap2*$^{\pm}$ mice crossing, and identified by genotyping on P21. As described in Li Jiada's paper [44], genotyping was performed using the genomic DNA collected from mouse tail, which was amplified using PCR to detect the ~ 39-base pair deletion in *Cntnap2*$^{\pm}$ and *Cntnap2*$^{-/-}$ offspring (Fig. S1). For generation of VPA-induced autism model mice, male and female C57BL/6 J mice were obtained from the PKUHSC animal breeding facility. On E12.5, pregnant dams were randomly assigned to two groups, VPA or saline, and intraperitoneally injected with VPA (Sigma; dissolved in physiological saline) at a dose of 600 mg/kg or equivalent volume of physiological saline. After weaning, male litters were separately kept and investigated in this study.

PLX5622 preparation and administration

PLX5622, a CSF1R inhibitor, was synthesized through six steps from commercially available compounds 2-amino-6-fluoropyridine, 5-fluoro-2-methoxypyridine-3-carbaldehyde and 3-iodo-5-methyl-1-(triisopropylsilyl)-1H-pyrrolo [2,3-b] pyridine, following the reference [32]. The optimized PLX5622-fumaric acid salt (PLX5622-FA) was formed by heating to reflux of PLX5622 and fumaric acid in methyl ethyl ketone. The final product PLX5622-FA, 6-fluoro-N-((5-fluoro-2-methoxypyridin-3-yl) methyl)-5-((5-methyl-1H-pyrrolo[2,3-b] pyridin-3-yl) methyl) pyridin-2-amine (fumaric acid salt), was validated using nuclear magnetic resonance spectroscopy (NMR) for chemical structure and high-performance liquid chromatography (HPLC) for purity (Fig. S2–S4). The chow containing PLX5622 at a concentration of 1200 ppm and the normal chow (control) were prepared by Jiangsu Xietong Biological Co., Ltd (Jiangsu, China). Briefly, PLX5622 drug chow was made by homogeneously blending PLX5622-FA powder with AIN-93 diet according to the company's proprietary procedures. For microglial depletion and repopulation, mice were fed with PLX5622-containing chow from P21 to P31, followed by normal chow for the remainder of the study.

Three-chamber social interaction test

The test apparatus was a rectangular, white acrylic box with three dimensions of 60 cm in length, 40 cm in width and 25 cm in height. The box was divided into three chambers with each one 20 cm long, and the dividing walls have a 10 cm opening in the center which allows test mice to freely access to three chambers. Placed in the center of each side chamber was a metal cylinder (10 cm diameter × 15.5 cm height) with its wall composed of 12 thin metal rods (~ 1 cm apart between two rods), which allows olfactory, visual, auditory contacts between internal and external mice. The apparatus together with the cylinders were washed and cleaned using 70% (v/v) ethanol after each trial. Before the test session, subject mouse was placed in the center chamber of the apparatus and allowed to habituate all chambers for 5 min. In the first phase of test session, an unfamiliar male C57BL/6 J mouse of same age (Stranger 1) was randomly placed in one cylinder, while a black Object with similar size was placed in the other cylinder. The test was started by placing subject mouse in the central chamber, and allowed to explore the chambers freely for 10 min. In the second phase, the Object was replaced with a novel strange male C57BL/6 J mouse (Stranger 2), and the subject mouse was allowed to explore the whole apparatus freely for 10 min. Time spent in sniffing the Object or strange mice was recorded by a computer-linked overhead video camera and analyzed using Smart v3.0 software.

Reciprocal social interaction test

Subjected mice were individually placed in a clean, white acrylic box ($40 \times 20 \times 30$ cm^3) with an unfamiliar conspecific matched mouse according to genotype, age, sex, and treatment. The mice were allowed to interact with each other freely for 5 min. Time spent in social interactions, including close following, physical touching, nose-to-nose sniffing, nose-to-anus sniffing, and crawling over/under each other, were recorded and analyzed manually in a blinded manner.

Self-grooming test

Tested mice were individually placed in a mouse home cage without bedding for 20 min. Grooming duration of each mouse during the last 10 min was manually analyzed by an observer blind to the treatment.

Nest building

Nest building test was carried out in clean mouse home cages. The cages were individually sterilized and supplemented with fresh, unscented mouse bedding. Subjected mice were individually placed in a cage and allowed to acclimate for 6 h. A corresponding number of commercially available cotton fiber nestlets ($5.0\times5.0\times0.5$ cm^3, ~ 2.5 g each, Ancare) were separately weighed on an analytical balance. Next, a nestlet was placed on top of the bedding in the test cage, and the mouse was left undisturbed for further 16 h. After test completion, test mice were moved to a clean cage and the final nest were documented without disturbing. Nest building was scored following a definitive 5-point nest-rating scale [45]. During the whole process of test, mice were allowed to freely access to chow and water.

Marble-burying test

Marble-burying test was performed in non-transparent acrylic cages ($20\times30\times40$ cm^3) filled with free, unscented bedding material to a 5-cm depth. Prior to the test, 20 glass toy marbles (assorted colors, 14 mm in diameter) were gently placed on the surface of the bedding in five rows of four marbles, which were evenly set at 5-cm intervals. Subjected mice were individually placed into the corner of the test cage and remained undisturbed for 30 min. After test completion, mice were removed and returned to the home cage. The number of buried marbles was manually calculated in a blind manner. A marble was scored as buried if two-thirds of its surface area is covered by bedding.

Open field locomotion test

The open field test was carried out in a non-transparent square cage ($50\times50\times50$ cm^3). Each subjected mouse was placed in the center of the open field arena and allowed to freely explore for 15 min. Mouse movements were recorded by a computer-linked overhead video camera. Data including total distance traveled and time spent in different area were analyzed using Smart v3.0 software.

Immunostaining for microglia

For histology and morphological analysis of microglia, mice were anesthetized and transcardially perfused with physiological saline followed by 4% (w/v) paraformaldehyde (PFA). Next, brains were removed, washed using PBS, and fixed in PFA solution for further 6 h. The fixed brains were cryopreserved in 30% (w/v) sucrose solution for 72 h, and embedded in optimal cutting temperature (OCT) compound (Sakura, Japan). Coronal Sects. (45 μm thick) were cut using a cryostat microtome (Leica CM3050S). Brain sections were allowed to rewarm at room temperature and rinsed three times using PBS. Next, sections were incubated in 0.5% (v/v) Triton X-100 in PBS for 30 min, and then blocked in 5% (w/v) BSA and 0.1% (v/v) Triton X-100 in PBS for 2 h. The blocked sections were then reacted with the rabbit anti-mouse IBA1 primary antibody (1:1000; Wako, 019–19741) or the rabbit anti-PDGFRα primary antibody (1:300; CST, 3174) at 4 °C overnight. Following five PBS-washes, sections were incubated with Alexa Fluor 488-conjugated goat anti-rabbit IgG secondary antibody (1:1000; Jackson, ZF0511) or Alexa Fluor 594-conjugated goat anti-rabbit IgG secondary antibody (1:1000; Jackson, ZF0516) for 2 h at room temperature. Sections were then washed for three times, counterstained with Hoechst 33,342 (Sigma-Aldrich), and mounted with glass coverslips.

Images of the whole brain sections were scanned using Vectra Polaris 1.0 (PerkinElmer), and images of somatosensory cortex, hippocampal CA1 and striatum regions were taken using a confocal microscope (Zeiss LSM 880) with a×40 objective at multiple z-planes. Both maximum projection of the image stacks and a slice-by-slice view were used to ensure the continuity of microglial branches. Microglial morphology analysis and rendering were performed using Bitplane Imaris 9.9 software. For comparison between the same autism-model mice, all stained images were taken for comparable sections of issue from each mouse, collected with the same laser settings, and processed by automated analysis using the same spot, surface or filament modules from Bitplane Imaris 9.9.

Golgi staining for neurons

Golgi-Cox impregnation of neurons was carried out using the FD Rapid Golgi Stain Kit (FD Neuro Technologies, Columbia, USA) following the manufacturer's instructions. Briefly, mice were euthanized, and brains were dissected immediately and rinsed using PBS. Next, the brains were immersed in a mixture of FD Solution A and Solution B for 14 d in darkness at room temperature, and then transferred to FD Solution C and kept for 72 h in the dark. Coronal Sects. (150 μm thick) were cut using a Leica cryostat microtome, mounted on gelatin-coated slides, and dried overnight. The sections were then immerged in FD Solution 2 (a mixture of Solution D and Solution E) for 10 min. After three water-washes, the slides were successively dehydrated in 50%, 70%, 95%, and 100% alcohol, and then cleared in Xylene three times. Neurons were imaged using a confocal microscope (Zeiss

LSM 880) with a × 63 oil objective at multiple z-planes. Counting and morphometrical analysis of spines was performed using Bitplane Imaris 9.9 software.

Statistical analysis

Statistical analyses, including one-way ANOVA and two-way ANOVA with Sidak's, Bonferroni's or Tukey's post hoc multiple comparisons test, as well as Student's t test, were performed using the software Graphpad Prism 8.0. Data are presented as raw means ± standard error of the mean (SEM). For all analyses, statistical significance was accepted at $p < 0.05$, and statistical trend was considered at $p < 0.1$. The results of statistical analyses are summarized in Table S1.

Results

PLX5622 alleviates behavioral deficits in *Cntnap2* KO mice

We first investigated pharmacological effects of PLX5622 on behaviors of *Cntnap2* KO mice. As shown in Fig. 1A, the mice in this experiment were divided into four groups: WT, WT + PLX5622, KO and KO + PLX5622. The WT and KO groups belonged to the control chow treatment groups ("control") that were fed with a control chow from P21-P80; the WT + PLX5622 and KO + PLX5622 were the "microglial depletion and microglial repopulation" groups, which were fed PLX5622-containing chow from P21-P31, followed by control chow for the remainder of the study. Behavioral tests were carried out from P70-P80.

As reported by Penagarikano [42], *Cntnap2* KO mice show social behavior abnormalities. Firstly, we performed a three-chamber social interaction test to evaluate PLX5622 effect on sociability and social novelty. In the first phase of the test, WT and WT + PLX5622 mice had significantly longer duration of sniffing time spent with Stranger 1 mouse than that with an Object, indicating that they had normal sociability and PLX5622 didn't alter the sociability of WT mice (Fig. 1B). Meanwhile, *Cntnap2* KO mice failed to show good sociability, specifically, there was no significant difference in the sniffing time that KO mice spent with Stranger 1 or the Object. However, PLX5622 significantly increased sniffing time between the KO mice and Stranger 1, indicating that PLX5622 can significantly improve the sociability

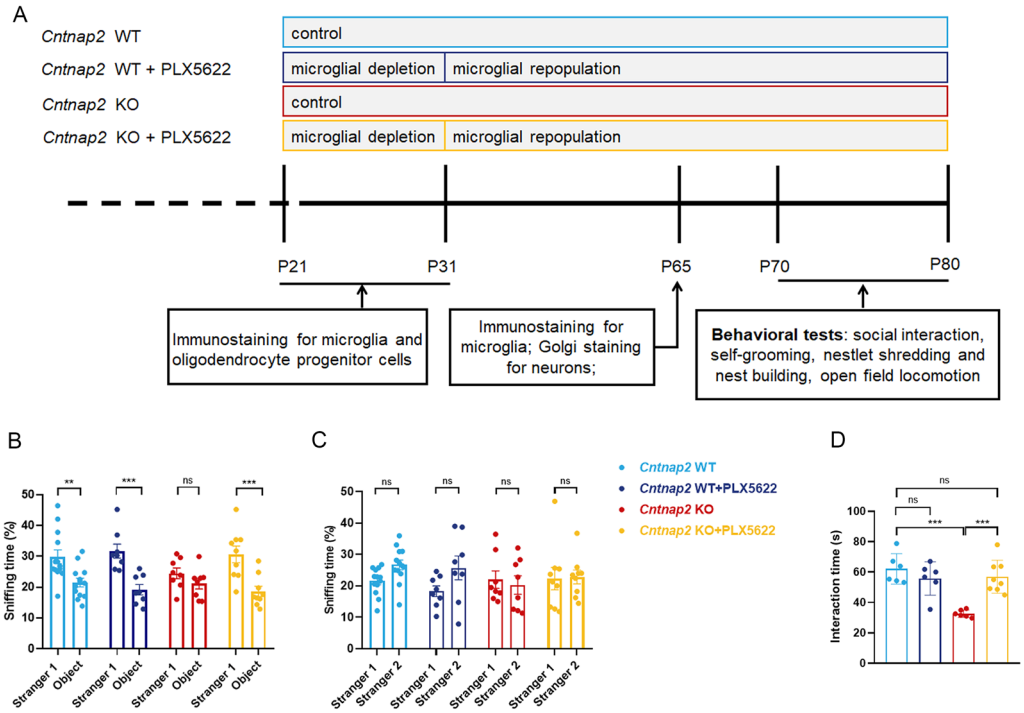

Fig. 1 PLX5622 rescues social behavioral deficits in the *Cntnap2* KO mice. **A** Experimental timeline. After weaning on P21, 3–5 *Cntnap2* WT and KO pups were sacrificed for histological test, while others were supplied with PLX5622 (1200 ppm) or normal chow (control) for 10 days, following which mice were returned to normal chow for the remainder of the study. One cohort of mice were killed at P31 or P65, and brain tissues were collected for histological test. Another cohort of mice underwent a battery of behavioral tasks at P70-P80. **B**, **C** Three-chamber social interaction test for four groups of *Cntnap2* WT and KO mice treated or not treated with PLX5622 (as labeled in the inset of (**C**). Sniffing time with Stranger 1 and Object in phase 1 (**B**); sniffing time with Stranger 1 and Stranger 2 in phase 2 (**C**). n = 8–13 per group; two-way ANOVA for (**B**) and (**C**). **D** Reciprocal social interaction test for all groups. n = 6–8 per group; one-way ANOVA. ***$p < 0.001$; **$p < 0.01$; "ns" denotes no significance. Data are expressed as mean ± SEM

of *Cntnap2* KO mice. In the second phase of the three-chamber test (Fig. 1C), WT mice exhibited a clear preference for interacting with a novel social partner (Stranger 2) rather than with a familiar one, whereas KO mice didn't display a notable preference for a new partner, supporting that *Cntnap2* KO mice can be used as a model for studying social novelty [42, 46]. However, compared with KO mice, KO + PLX5622 mice spent more time interacting with Stranger 2. Although this improvement did not reach a statistically significant difference, PLX5622 did show a tendency to improve social novelty behavior in *Cntnap2* KO mice. Secondly, we carried out reciprocal social interaction tests, which have also been utilized for assessment of spontaneous social behaviors in various rodent species [47]. As shown in Fig. 1D, compared with WT mice, WT + PLX5622 mice did not have significantly less time in interacting with intruders, suggesting that PLX5622 can't affect spontaneous social behaviors of WT mice. Clearly, KO mice had significantly less social interaction time than WT mice. But no significant difference was observed in reciprocal interaction time of WT and KO + PLX5622 groups (Fig. 1D). These results demonstrated that PLX5622 can effectively improve reciprocal social behavior of KO mice.

We next performed a battery of non-social behavioral tests. First, in the open field test, we found that the four groups of mice spent well-matched total time in the periphery or center of the arena (Fig. 2A). In concordance with a previous report [42], *Cntnap2* KO mice displayed significantly increased locomotor activity than their WT counterparts (Fig. 2B). PLX5622 treatment effectively reduced the locomotor velocity and alleviated the hyperactive behavior of *Cntnap2* KO mice, but had no negative effect on the locomotor activity of WT mice. Second, we explored grooming behaviors of the test mice, which can provide an index of repetitive/stereotypic behavior in rodents [47]. Similar to a previous report [42], KO mice spent more time in self-grooming than WT mice (Fig. 2C). WT + PLX5622 and WT mice spent comparable time in self-grooming, while KO + PLX5622 had significantly less time in this repetitive behavior than KO did. These observations demonstrate that PLX5622 can effectively alleviate repetitive behavior of KO mice, but almost had no effect on WT mice. Third, we performed nest building test, in which the test mice first shredded a tightly packed square nestlet and then arranged it into a nest [45, 48]. As shown in Fig. 2D, E, compared with KO mice, the nesting behavior of *Cntnap2* KO mice was significantly impaired, and the nesting score was less than half of WT mice. PLX5622 treatment significantly improved the scores earned by KO mice and did not impair scoring of WT mice (Fig. 2E).

In summary, PLX5622 not only alleviates autism-like core symptoms (social deficits and repetitive behaviors)

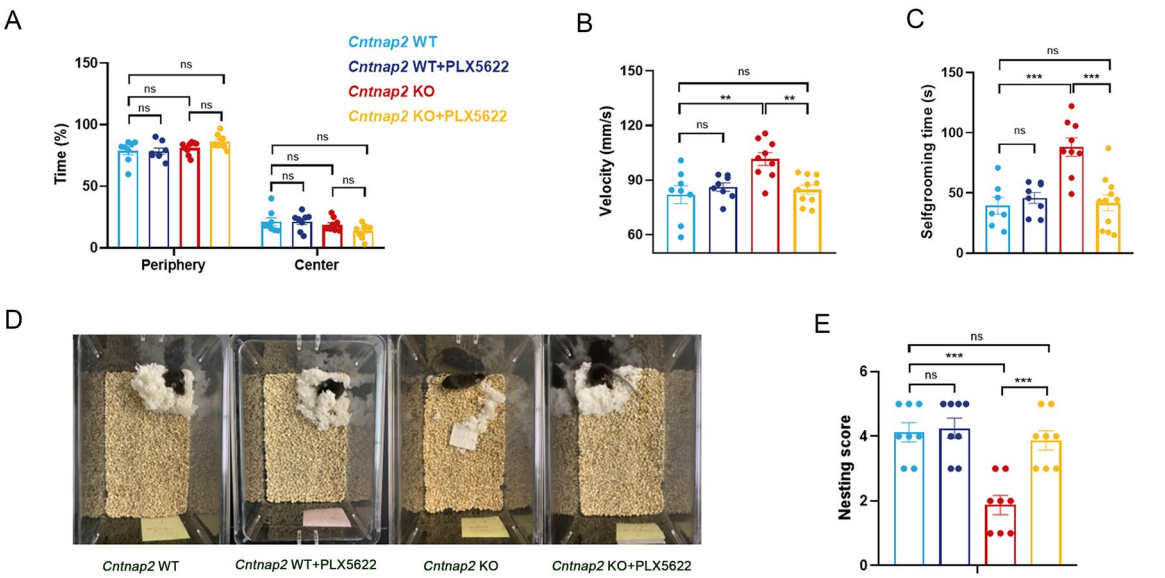

Fig. 2 PLX5622 alleviates hyperactivity and abnormal grooming, and improves nesting behavior of the *Cntnap2* KO mice. **A**, **B** Open field test. Time spent in center and periphery zone (**A**) and velocity (**B**) for four groups of *Cntnap2* WT and KO mice treated or not treated by PLX5622. Two-way ANOVA for (**A**) and one-way ANOVA for (**B**); n = 8–10 per group. **C,** Time spent in self-grooming by four groups of mice as labeled in (**A**). One-way ANOVA; n = 7–11 mice per group. **D**, **E** Nesting behavior test. Nestlets after test were documented for all tested animals (**D**). Scoring was performed using grades ranging from 1 (very poor) to 5 (optimal): grade 1 corresponds to an untouched nestlet, while grade 5 means nestlet fully shredded to form a crater-like, delimited nest (**E**). One-way ANOVA; n = 8 mice per group. ***$p < 0.001$; **$p < 0.01$; "ns" denotes no significance. Data are expressed as mean ± SEM

in *Cntnap2* KO mice, but also mitigates their hyperactivity and improves their nest-building ability. In line with previous findings that global depletion of microglia resulted in no change in sociability behavior of wild-type C57BL/6 mice [27, 29, 39], PLX5622 hardly altered behaviors of *Cntnap2* WT mice (Figs. 1, 2). Noteworthy, PLX5622 can successfully correct social and repetitive behavior deficits of MIA model mice without affecting behaviors, microglia and neuronal spine morphology of the saline group [38]. Therefore, in the following experiments, we didn't set up the group of wild type or control mice treated with PLX5622 so that as less as mice would be sacrificed.

PLX5622 restores microglial number and morphology in *Cntnap2* KO mice to the level of wild type

To obtain insights into the cellular mechanisms underlying PLX5622-alliviating autism-like behaviors in *Cntnap2* KO mice, we compared microglial number and morphology in different brain regions of *Cntnap2* WT, KO and KO + PLX5622 groups of mice on P65 using immunofluorescence for IBA1. Compared with WT mice, the number of microglia in somatosensory cortex of *Cntnap2* KO mice significantly increased; correspondingly, microglia in KO mice presented amoeboid-like phenotype with decreased process area, decreased length and number of process branches, and increased cell body (Fig. 3 A-F). PLX5622 administration significantly decreased microglial number, increased process area, length and number, and had tendency in decreasing cell body size in somatosensory cortex of *Cntnap2* KO mice, to a level of WT mice (Fig. 3A–F). Different from the case of somatosensory cortex, *Cntnap2* KO mice showed no abnormalities in microglial number, cell body volume and branch number in the CA1 region compared with WT mice (Fig. 3G–L). Noteworthy, microglial process area and length in the CA1 of KO mice were significantly smaller than that in WT mice, and this difference was

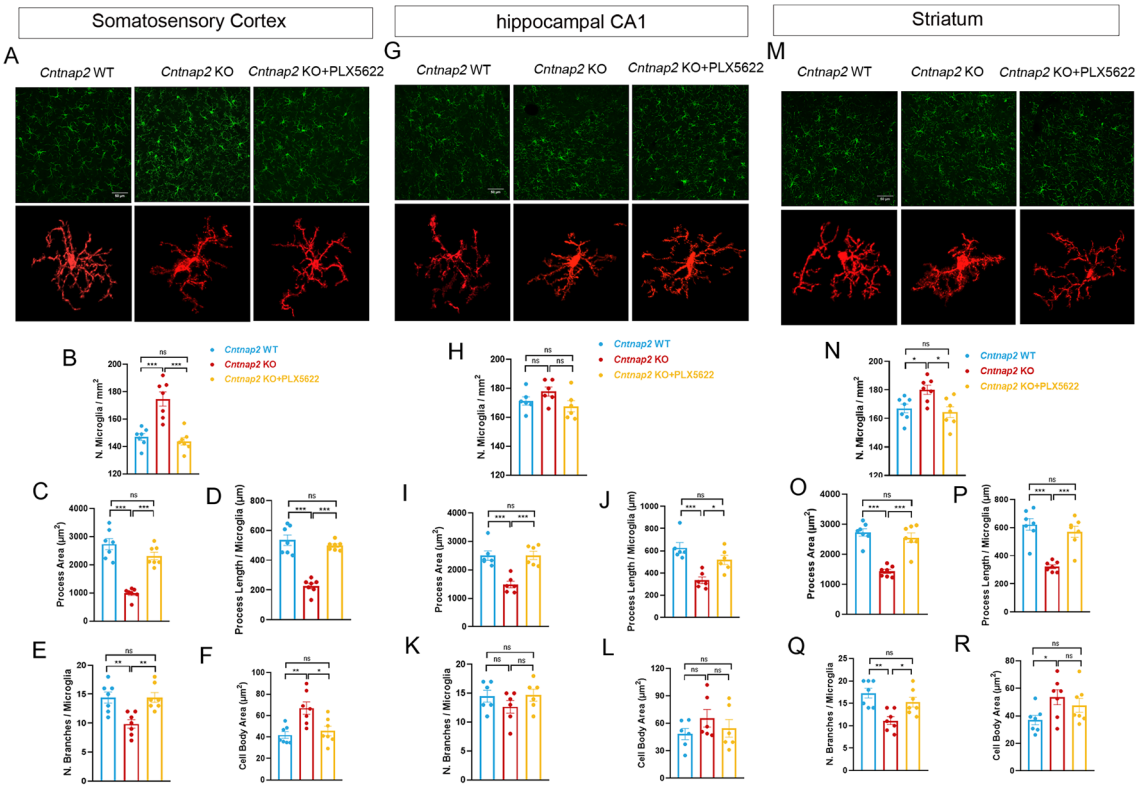

Fig. 3 PLX5622 restores microglial number and morphology in the somatosensory cortex (**A**–**F**), hippocampal CA1 (**G**–**L**) and striatum (**M**–**R**) of the *Cntnap2* KO mice. **A**, **G**, **M**, Representative immunofluorescence images of IBA1$^+$ microglia (top) and representative microglia images reconstructed by Imaris 9.9 (bottom) in the somatosensory cortex (**A**), hippocampal CA1 (**G**) and striatum (**M**) of three groups of *Cntnap2* WT, KO or PLX5622-treated KO mice. Scale bar: 50 μm; n = 3–5 mice for each group. **B-F**, **H–L**, **N-R**, Statistical analysis of the number and morphology of microglia in the somatosensory cortex (**B**–**F**), hippocampal CA1 (**H**–**L**) and striatum (**N–R**) in the three groups. Comparison of microglia numbers in 1 mm^2 (**B**, **H**, **N**), microglial process area (**C**, **I**, **O**), microglial process length (**D**, **J**, **P**), number of branches per microglia (**E**, **K**, **Q**), and microglial cell body area (**F**, **L**, **R**) in each group. n = 6–7 cells per group; one-way ANOVA. ***$p < 0.001$; **$p < 0.01$; *$p < 0.05$; "ns" denotes no significance. Data are expressed as mean ± SEM

obviated by PLX5622 (Fig. 3G–L). Like the case of the somatosensory cortex region, compared with WT mice, microglial number and cell body volume in the striatum of *Cntnap2* KO mice significantly increased, whereas microglial process area, length and branch number significantly decreased (Fig. 3M–R). PLX5622 effectively reversed such changes of microglia in the striatum of *Cntnap2* KO mice to the WT level (Fig. 3M–R). In conclusion, PLX5622 administration can reverse the changes in the number and morphology of microglia in somatosensory cortex, hippocampal CA1 and striatum of *Cntnap2* KO mice.

PLX5622 corrects dendritic spine abnormalities in the striatum region of *Cntnap2* KO mice

To investigate whether microglial variation occurs alongside neurophysiological alteration, we detected density and morphology of dendritic spines in the above mentioned three brain regions of *Cntnap2* WT, KO and KO + PLX5622 groups of mice on P65 using Golgi staining. As shown in Fig. 4A–H, there was no significant difference in the density and morphology of dendritic spines in the somatosensory cortex and hippocampal CA1 between *Cntnap2* KO and WT mice. PLX5622 did not affect dendritic spines in the somatosensory cortex and hippocampal CA1 of *Cntnap2* KO mice (Fig. 4A–H). In contrast, the density as well as the proportions of mushroom-shaped and stubby dendritic spines in the striatum of *Cntnap2* KO mice significantly decreased in comparison with WT mice (Fig. 4I–L). Such neurophysiological abnormalities in the striatum of KO mice were rescued by PLX5622 to the level of WT (Fig. 4I–L).

PLX5622 ameliorates behavioral deficits in VPA-model mice

The mice in this experiment were divided into three groups: saline, VPA, VPA + PLX5622 (Fig. 5A). The VPA + PLX5622 mice were provided with PLX5622 (1200 ppm) diet on P21 for 10 days, and then returned to normal chow. At the indicated time points, different cohorts of mice were sacrificed for histological studies or kept alive for a battery of behavioral tasks (Fig. 5A). Here are the results of behavioral test. Briefly, PLX5622 can

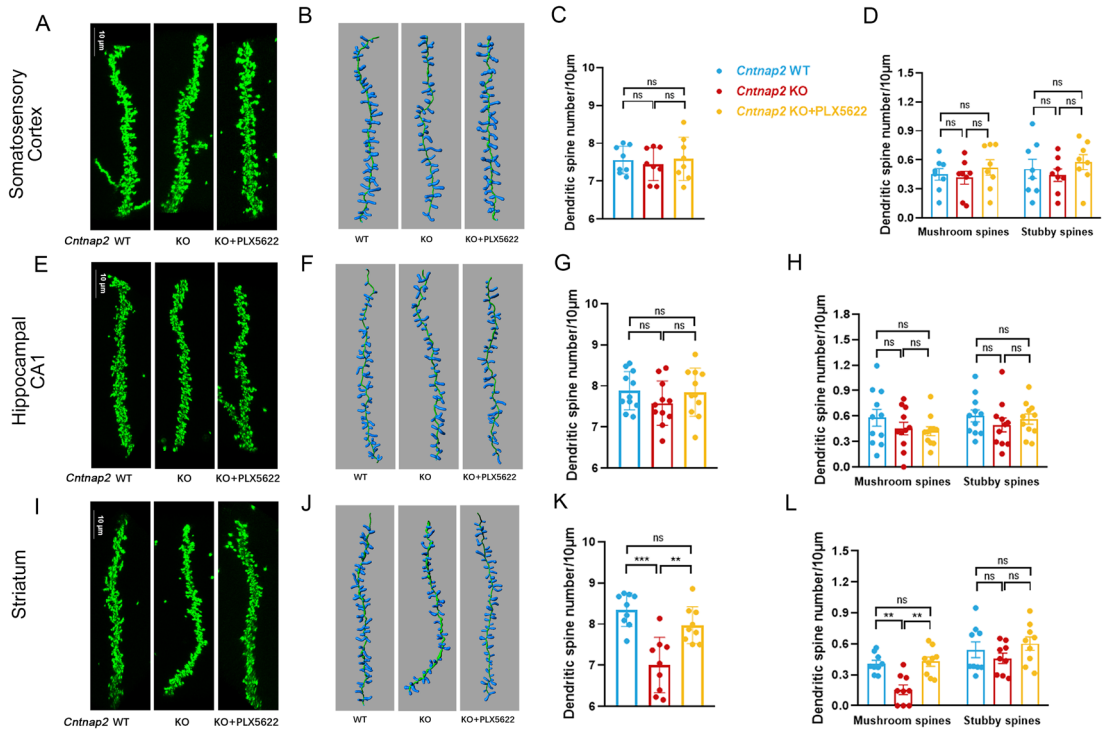

Fig. 4 Description and statistical analysis of dendritic spine density and morphology of neurons in the somatosensory cortex (A-D), hippocampal CA1 (E–H), and striatum (I-L) of three groups of mice: Cntnap2 WT, KO mice and PLX5622-treated KO mice. **A**, **E**, **I**, Representative images of dendritic spines of the somatosensory cortex (**A**), hippocampal CA1 (**E**), and striatum neurons (**I**). Scale bar: 10 μm; n = 3–5 mice per group. **B**, **F, J**, Representative 3D image of dendritic spines reconstructed by Imaris 9.9 for (**A**), (**E**) and (**I**), respectively. **C**, **G**, **K**, Statistical analysis of the total number of dendritic spines contained in 10 μm dendrites. n = 8–11 cells per group; one-way ANOVA. **D**, **H**, **L**, Statistical analysis of the number of mushroom and stubby dendritic spines contained in 10 μm dendrites. n = 8–11 cells per group; two-way ANOVA. ***$p < 0.001$, **$p < 0.01$, *$p < 0.05$, "ns" denotes no significance. Data are expressed as mean ± SEM

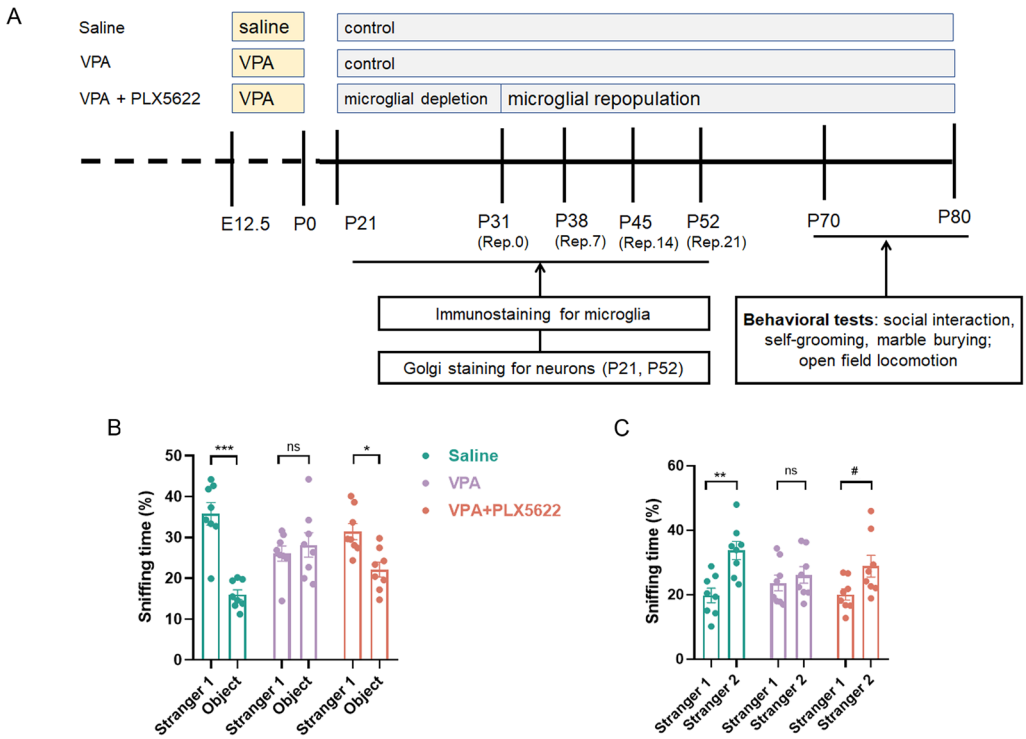

Fig. 5 PLX5622 corrects social behavioral deficits in VPA model mice. **A** Experimental timeline. C57BL/6 J female mice received VPA or saline injection on E12.5, and the prenatally saline-treated male offspring were assigned to the "Saline" group. The VPA-treated male offspring were randomly divided into two groups: one group provided with normal diet ("VPA" group); the other group reared with PLX5622 diet at P21 for 10 days and then with normal chow ("VPA + PLX5622" group). One cohort of mice were sacrificed respectively at P21, P31, P38, P45 and P52 for histological analysis, while a separate cohort of mice received a battery of behavioral tests at P70-P80. The "VPA + PLX5622" group of mice that underwent 0, 7, 14 and 21 days of microglia repopulation after withdraw of PLX5622 at P31 were hereinafter categorized as "VPA Rep.0", "VPA Rep.7", "VPA Rep.14" and "VPA Rep. 21" group, respectively. **B-C,** three-chamber social interaction test for the Saline, VPA and VPA + PLX5622 groups of mice. Sniffing time with Stranger 1 and Object in phase 1 (**B**); sniffing time with Stranger 1 and Stranger 2 in phase 2 (**C**). n = 8 per group; two-way ANOVA. ***$p < 0.001$; **$p < 0.01$; *$p < 0.05$; $^{\#}p < 0.1$, "ns" denotes no statistical significance. Data are expressed as mean ± SEM

effectively rescue social deficits and stereotypical repetitive of the VPA model mice.

In the first phase of three-chamber social interaction test, the saline group of mice had significantly longer time in Stranger 1 over Object, whereas the VPA model mice spent comparable time in sniffing with Stranger 1 and Object (Fig. 5B). Meanwhile, compared with the saline group, VPA model mice spent less time in sniffing with Stranger 1 (Fig. 5B). These results demonstrate that the VPA model mice have impaired sociability. Similar to the saline group, the PLX5622-treated VPA model mice had significantly longer time in Stranger 1 over Object (Fig. 5B), indicating that PLX5622 can ameliorate their deficits in sociability. In the second phase of the test (Fig. 5C), the saline group of mice spent significantly more time in the new comer (Stranger 2), and the VPA model mice did not show statistical difference in the sniffing time spent with Stranger 1 or Stranger 2, indicating that VPA model mice have damaged social novelty. PLX5622 can effectively improve the social novelty of VPA model mice, as showed by a trend of increased sniffing time with the new comer (Fig. 5C).

In open field test (Fig. 6A), compared with the saline group, the VPA model mice spent significantly less time in the center arena and more time in the periphery area, indicating that the VPA model mice have more intensive anxiety. PLX5622 hardly alleviated anxiety of the VPA model mice, since it didn't alter their time in the center arena (Fig. 6A). In addition, there was no significant difference in the total movement distance among the three groups, indicating that VPA or PLX5622 treatment did not affect locomotor activity of mice (Fig. 6B).

In self-grooming test (Fig. 6C), the VPA model mice showed more frequent and continuous grooming behavior, and their total self-grooming time was nearly twice that of the saline group. PLX5622 treatment significantly reduced the self-grooming time of the VPA model mice to the level of the saline group (Fig. 6C). In addition, marble burying test was carried out to evaluate stereotypical repetitive behavior in all groups. Compared with

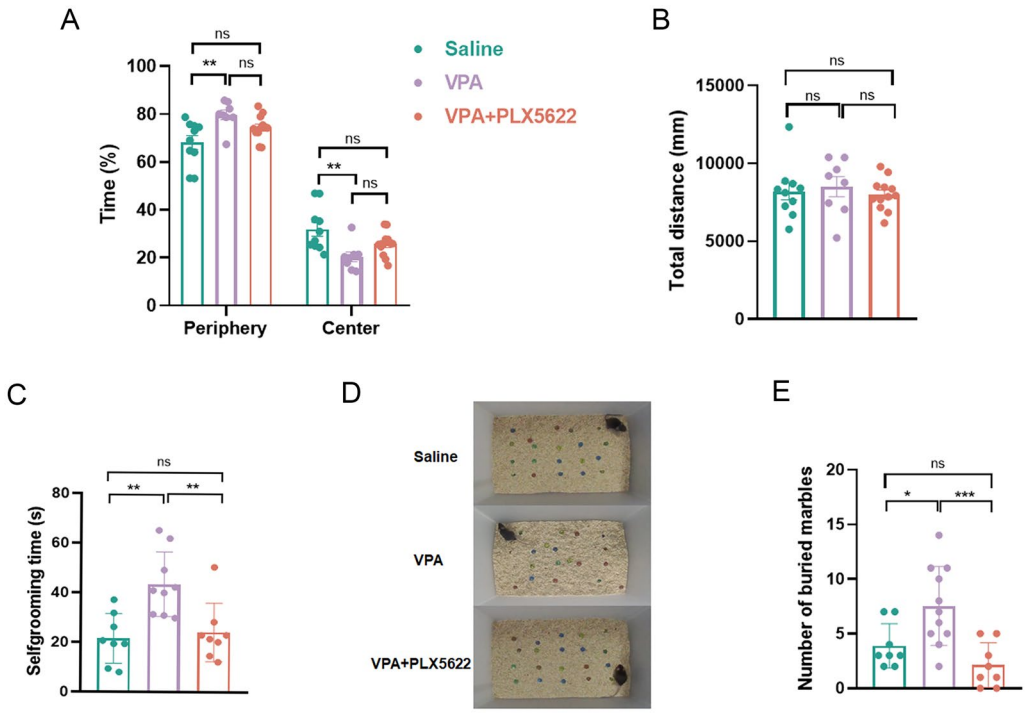

Fig. 6 PLX5622 alleviates anxiety and repetitive behavioral deficits in VPA-model mice. **A**, **B** Open field test. Time spent in center and periphery zone (**A**) and total distance (**B**) during test for three groups of mice: saline, VPA and VPA + PLX5622. Two-way ANOVA for (**A**) and one-way ANOVA for (**B**); n = 8–12 per group. **C**–**E,** Repetitive behavior was evaluated by the time spent in self-grooming (**C**), and number of buried marbles in marble burying test (**D**, **E**). One-way ANOVA for (**C**) and **E** n = 8–11 per group. ***$p < 0.001$; **$p < 0.01$; *$p < 0.05$; "ns" denotes no statistical significance. Data are expressed as mean ± SEM

the saline group, the VPA model mice buried significantly more marbles in the test (6.8 ± 3.0 versus 2.7 ± 1.8) (Fig. 6D, E). However, there was no statistically significant difference in the number of marbles buried by the VPA + PLX5622 and saline groups, indicating that PLX5622 significantly alleviated stereotypical marble-burying behavior of the VPA model to the level of the saline group.

PLX5622 induces microglia depletion and repopulation in the VPA model mice

To investigate how PLX5622 affects microglial dynamic change in depletion and repopulation, we detected microglial number and morphology in the above mentioned three brain regions of the 'Saline', 'VPA' and 'VPA + PLX5622' groups at the indicated time points via using immunofluorescence for IBA1 (Fig. 5A). In line with a previous report that prenatal VPA exposure changed microglial phenotypes from resting to activated states in the prefrontal cortex and hippocampus regions of infant VPA model rats [17], we observed that microglia underwent a similar phenotypic change in the somatosensory cortex, hippocampal CA1 and striatum regions of the VPA model mice (Figs. 7, 8, 9). Concretely speaking, in comparison with the Saline P21 group of mice, the VPA model mice on P21 presented decreased process area, length and branch number and increased cell body volume, indicating microglia morphology abnormalities in the three brain regions (Figs. 7, 8, 9). Noteworthy, microglial number increased in the hippocampal CA1 region of the VPA model mice, further indicating microglial abnormality in this brain region (Fig. 8).

In general, PLX5622 led to a nearly identical process of microglia depletion in the somatosensory cortex, hippocampal CA1 and striatum regions of the VPA model mice. As shown in Figs. 7, 8, 9, 10 days of PLX5622 treatment eliminated ~ 90% of microglia in the three brain regions of the VPA model mice (VPA Rep.0), and left a small population of microglia exhibiting an enlarged cell body and retracted processes similar with that before PLX5622 treatment (VPA P21). Meanwhile, similar microglial repopulation processes occurred in the somatosensory cortex, hippocampal CA1 and striatum regions of the VPA model mice (Figs. 7, 8, 9). For clarity, the focus here is on the somatosensory cortex region. After a 7 days period of recovery, the total number of microglia in this region of the VPA Rep.7 group increased to a level

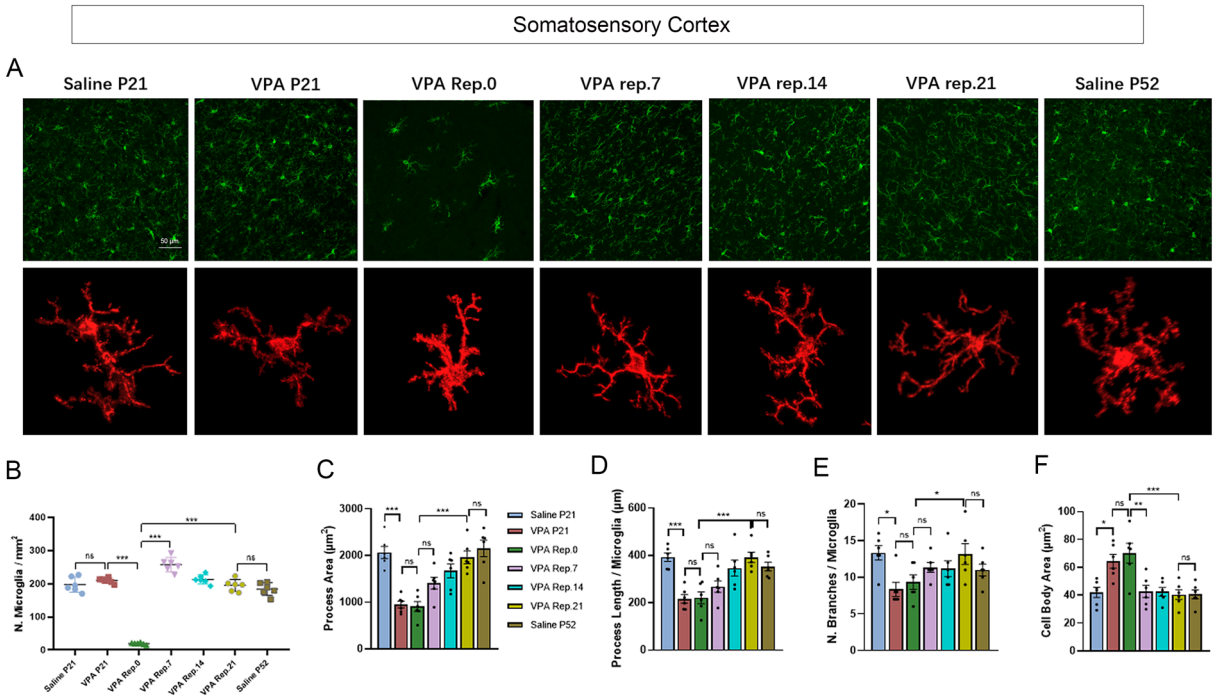

Fig. 7 Microglia depletion and repopulation in the somatosensory cortex of PLX5622-treated VPA-model mice. **A** Representative immunofluorescence images of IBA1$^+$ microglia (top) and representative microglia image reconstructed by Imaris 9.9 (bottom) in the somatosensory cortex in the seven groups of mice as indicated. n = 3 mice for each group. **B**–**F**, Statistical analysis of the number and morphology of microglia in the somatosensory cortex in each group: number of microglia (**B**), microglial process area (**C**), microglial process length (**D**), number of branches per microglia (**E**), and microglial cell body area (**F**). Scale bar: 50 μm; n = 6 cells per group; one-way ANOVA. ***$p < 0.001$; **$p < 0.01$; *$p < 0.05$; "ns" denotes no significance. Data are expressed as mean ± SEM

slightly higher than that before depletion (VPA P21), and microglia recovered to a resting state with significantly larger cell process area and branch number and smaller cell body volume in comparison with the VPA P21 group (Fig. 7). Noteworthy, microglial process length of the VPA Rep.7 mice had no significant difference with that of the VPA Rep.0 group. By the end of 14 days of recovery, the microglial number of the VPA Rep.14 group was close to the level of the VPA Rep.7 group, and the repopulated microglia were ramified (Fig. 7). After 21 days of recovery, microglial number, process parameters (area, length, and branch number) and cell body volume in the VPA Rep.21 group had significant difference with that in the VPA Rep.0 group, and however, didn't show any significant difference from those in the Saline group on P52 (Fig. 7). In the hippocampal CA1 and striatum regions of the VPA model mice (Figs. 8, 9), microglial number also swiftly restored to and maintained at a high level after 7 days of repopulation, and microglial morphology also underwent a gradual recovery with microglial process area, length and branch number increasing to a high level and cell body volume decreasing to a low level to the saline group on the 21th day after repopulation. Here we admit that we didn't have mouse in the VPA Rep.14 group for examining microglia in the striatum (Fig. 9). Nevertheless, it is conclusive that microglial repopulation in the striatum share a common dynamic process with those in the somatosensory cortex and hippocampal CA1 regions.

PLX5622 restores the number and morphology of dendrite spine in the VPA model mice

Compared with the saline group, the total number of dendritic spines in the somatosensory cortical region was significantly reduced in the VPA model mice on P21, and the number of mushroom-like dendritic spines was only about a quarter of that in the saline group (Fig. 10A–D). 21 days after removal of the PLX5622 diet (VPA rep.21), the total number of dendritic spines and mushroom-like dendritic spines restored to the level of the saline group. Noteworthy, the density of stubby dendritic spines had no significant difference between the saline and VPA groups. The density of dendritic spines in the hippocampal CA1 was significantly decreased in the VPA model mice on P21, and the number of both mushroom-like and stubby dendritic spines were significantly lower than those in the saline group. PLX5622 treatment effectively restored the number and morphology of dendritic spines

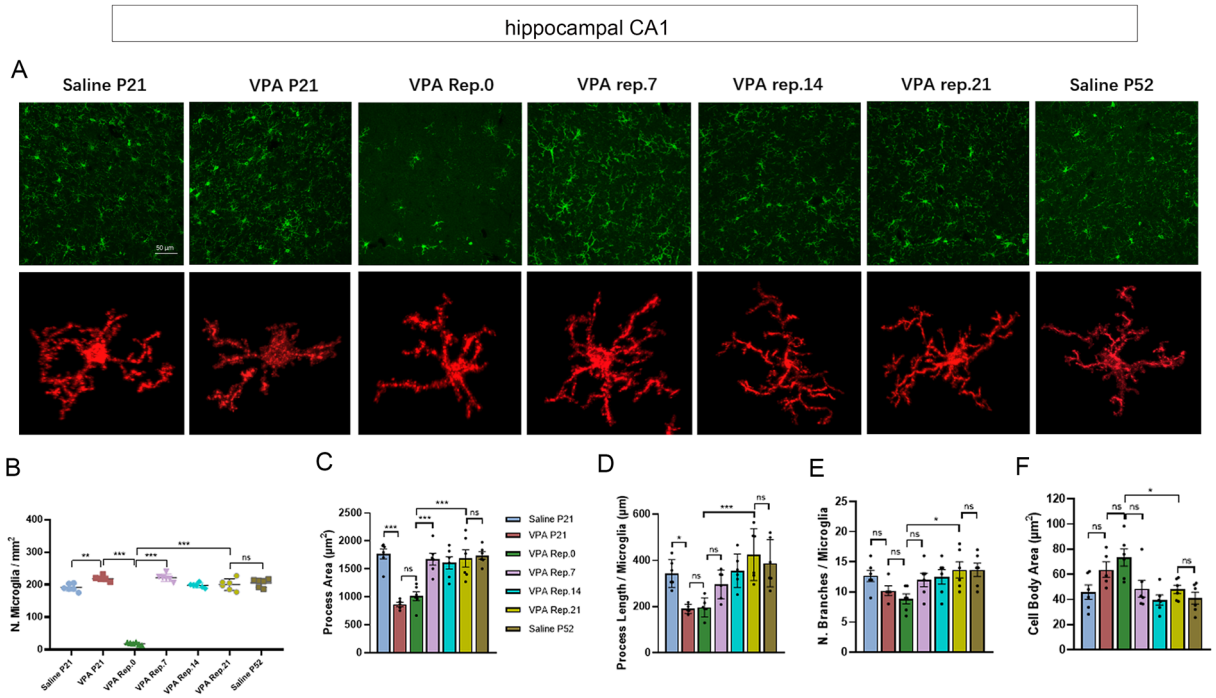

Fig. 8 Microglia depletion and repopulation in the hippocampal CA1 of PLX5622-treated VPA-model mice. **A** Representative immunofluorescence images of IBA1$^+$ microglia (top) and representative microglia image reconstructed by Imaris 9.9 (bottom) in the hippocampal CA1 in the seven groups of mice as indicated. n = 3 mice for each group. **B**–**F**, Statistical analysis of the number and morphology of microglia in the hippocampal CA1 in each group: number of microglia (**B**), microglia process area (**C**), microglia process length (**D**), number of branches per microglia (**E**), and microglia cell body area (**F**). Scale bar: 50 μm; n = 6 cells per group; one-way ANOVA. ***$p < 0.001$; **$p < 0.01$; *$p < 0.05$; "ns" denotes no significance. Data are expressed as mean ± SEM

in hippocampal CA1 of the VPA model mice (Fig. 10E–H). In the striatum, the density of total dendritic spines or stubby spines in the VPA-model group was also significantly lower than that in the saline group, and however, was higher than that in saline group upon PLX5622 correction (Fig. 10I–L). Expectedly, mushroom spine density in the VPA mice's striatum was significantly lower than that in the saline group, and rescued to the saline group level by PLX5622 treatment (Fig. 10I–L).

Discussion

Microglial depletion and repopulation through genetic targeting or pharmacological therapies (mainly with CSF1R inhibitors) exhibits great potential as an intervention in many neurological disease states [28, 34, 35, 49]. At present, there is only one study using CSF1R inhibitor-induced microglia depletion to intervene in behavioral abnormalities of MIA-invoked ASD model mice [38]. Considering high heterogeneity of ASD, we studied *Cntnap2* KO and prenatal VPA-exposure autism model mice to investigate how CSF1R inhibition may affect autism-like behavioral phenotypes induced by genetic or environmental risk factors, and how microglial depletion and repopulation occurs for behavioral modification.

Retrospective view of biological rationales or proofs for our experimental design

As shown in Figs. 1 and 5, only male offspring of ASD model mice were used in this study, and PLX5622, an CSF1R inhibitor, was used to eliminate microglia on P21 only for 10 days. The biological rationales or proofs underlying such an experimental design are elucidated as follows.

Firstly, why were only male offspring used? Despite striking heterogeneity in manifestation, ASD has a replicated feature that is the male preponderance with the male to female ratio around 4.5:1 [50]. Microglia demonstrate sexual dimorphism in their colonization, structure, function, and transcriptomic and proteomic profiles from early postnatal development onwards of rodents [51–53], and can sculpt sex differences in adult social behaviors likely owing to their prominent roles in sculpting neural circuit development [54, 55]. Lipopolysaccharide (LPS)-induced maternal immune activation has been reported to cause male-specific social deficits in *Cntnap2* KO mouse model for ASD [56]. Recent study has shown that sexual dimorphism in the social behavior of *Cntnap2* KO mice is associated with increased microglial activity and disrupted synaptic connectivity in the anterior cingulated

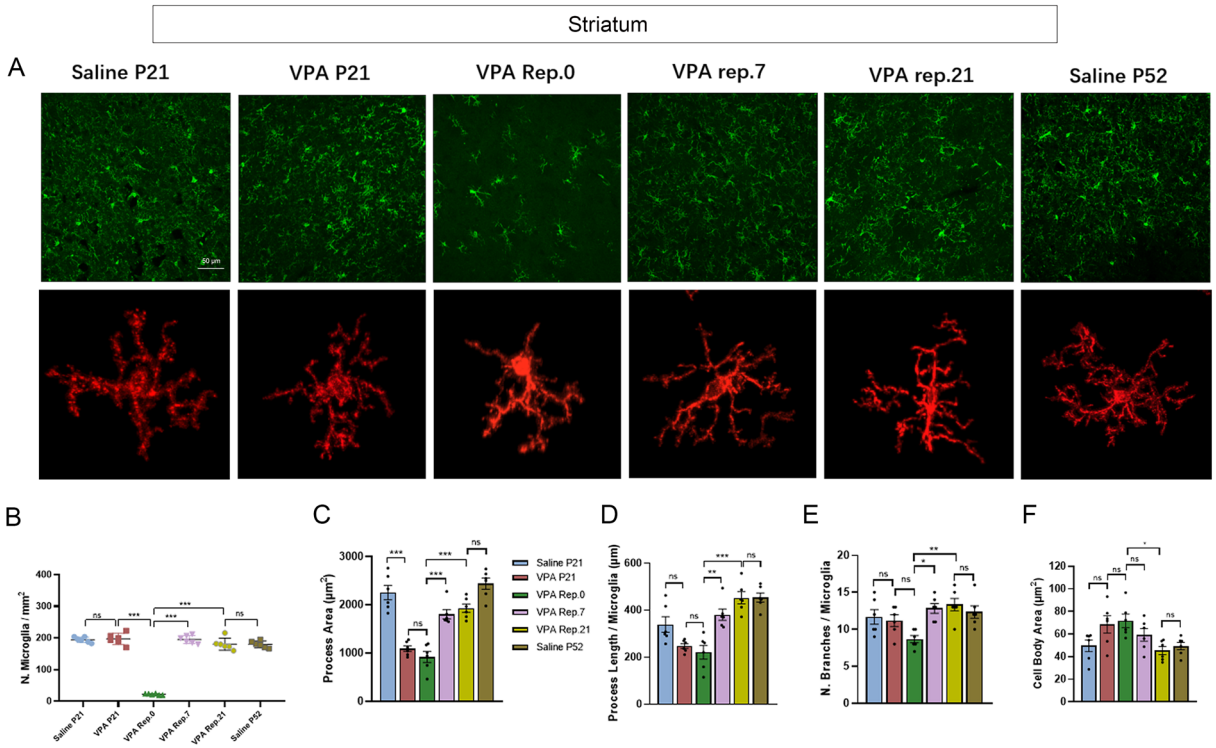

Fig. 9 Microglia depletion and repopulation in the striatum of PLX5622-treated VPA-model mice. **A** Representative immunofluorescence images of IBA1$^+$ microglia (top) and representative microglia image reconstructed by Imaris 9.9 (bottom) in the striatum in the six groups of mice as indicated. n = 3 mice for each group. **B**–**F**, Statistical analysis of the number and morphology of microglia in the striatum in each group: number of microglia (**B**), microglia process area (**C**), microglia process length (**D**), number of branches per microglia (**E**), and microglia cell body area (**F**). Scale bar: 50 µm; n = 6 cells per group; one-way ANOVA. ***$p < 0.001$; **$p < 0.01$; *$p < 0.05$; "ns" denotes no significance. Data are expressed as mean ± SEM

cortex [57]. Meanwhile, prenatal exposure to VPA led to male-specific alteration in synaptic development, morphological development and social interaction, while female offspring showed only marginal deficits [58–60]. Therefore, we used only male offspring of the two autism model mice in this study.

Secondly, why were microglia depleted in the time window from P21 to P31? In the rodent brain, microglia numbers peak at postnatal day 14 (P14), undergo a rapid decrease in the third postnatal week, and attain adult levels by P28 [61]. Furthermore, microglia exhibit an activated morphology and present high phagocytic activities during the postnatal three weeks in male rodent offspring [51]. It seems that postnatal three weeks is the critical time window for microglia to exert their functions in male rodents. Given that mice can take diet completely by themselves after weaning, we used CSF1R inhibitor-containing chow to rear male mice at P21 for lunching microglia depletion. The duration of microglia depletion in this study is 10 days from P21 to P31, half the duration of CSF1R inhibition in the MIA model that male and female mice were subjected to CSF1R inhibitor PLX5622 treatment from P21 to P42 [38]. Indeed, in comparison with male counterparts, female rodent offspring have more activated microglia with amoeboid morphology later in development (P30-P60) [51]. This observation likely underlies why longer duration of CSF1R inhibition till juvenile and adolescent stage was needed to deplete and repopulate microglia in female MIA model mice [38]. From this perspective, we think that microglia depletion for male *Cntnap2* KO or VPA model mouse doesn't need longer duration as in the MIA model. As shown in Fig. S5 and Fig. S6A, around 95% of microglia in male *Cntnap2* KO mice were depleted after 10 days of PLX5622 treatment from P21. At P21, male *Cntnap2* KO mice had significantly increased microglia number and significantly reduced microglia process area, process length and branch number in their somatosensory cortex area compared with male WT (Fig. S6). Unexpectedly, male *Cntnap2* KO mice had significantly reduced microglia number in their striatum region (Fig. S6D). Nevertheless, microglia in the striatum area of male *Cntnap2* KO exhibited shorter process and less branches (Fig. S6M–O). These data show that microglia in the male *Cntnap2*

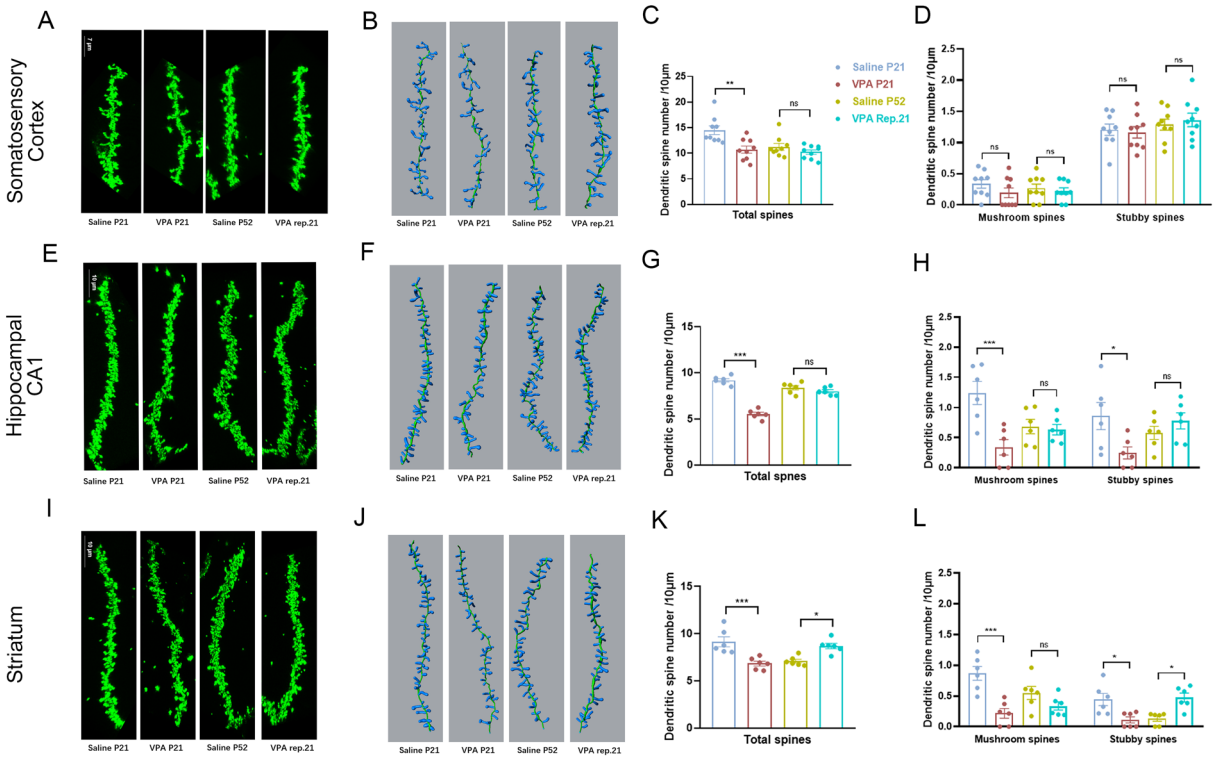

Fig. 10 PLX5622 treatment corrects dendritic spine density and morphology in the somatosensory cortex (**A**–**D**), hippocampal CA1 (**E**–**H**), and striatum (**I**–**L**) of the VPA-model mice. **A**, **E**, **I**, Representative images of dendritic spines in the somatosensory cortex (**A**), hippocampal CA1 (**E**), and striatum neurons (**I**) of four groups of mice: "Saline P21" (the Saline group of mice at P21), "VPA P21" (the VPA group of mice at P21), "Saline P52" (the Saline group of mice at P52) and "VPA rep. 21" (the PLX5622-treated VPA group of mice at P52). Scale bar: 7 μm (**A**) or 10 μm (**E** and **I**); n = 3 for each group. **B**, **F**, **J**, Representative 3D image of dendritic spines reconstructed by Imaris 9.9 for (**A**), (**E**) and (**I**), respectively. **C**, **G**, **K** Total number of dendritic spines contained in 10 μm dendrites. n = 6–9 per group; one-way ANOVA. **D**, **H**, **L** Statistical analysis of the number of mushroom and stubby dendritic spines contained in 10 μm dendrites. n = 6–9 per group; two-way ANOVA. ***$p < 0.001$, **$p < 0.01$, *$p < 0.05$. Data are presented as mean ± SEM

KO during the postnatal three weeks are more amoeboid-like with shorter pseudopodia, which endows microglia higher phagocytic activity [62]. As shown in Figs. 7, 8, 9, male VPA mice at P21 also had more amoeboid-like microglia compared with the saline group. These data also indicate that it is reasonable for us to launch microglia depletion at P21 for male *Cntnap2* KO and VPA mice in this study. However, a possibility is that earlier microglia depletion may also take effect, since a recent study shows that microglia in the anterior cingulate cortex of male *Cntnap2* KO at P8 and P14 present more activated state than WT mice [57]. A caveat is that microglia depletion at earlier stage and shorter duration may have limited effectiveness for ASD in clinical treatment.

Thirdly, why was PLX5622 selected as a pharmacological tool? Did PLX5622 affect other types of CNS cells like oligodendrocyte progenitor cells (OPCs)? The development, survival and proliferation of microglia depends on signaling of CSF1R [6, 27], a member of the class III receptor tyrosine kinases (RTKs) that also include KIT, PDGFRα, PDGFβ and Flt3 [63]. Among these members, PDGFRα is highly expressed by OPCs and PDGFRα kinase activity is essential for their survival [64]. Different from their diverse extracellular domains, the intracellular kinase domains of the class III RTKs have a highly conserved ATP-binding pocket that is targeted by PLX5622 and PLX3397, two commonly used CSF1R inhibitors for microglia depletion [29]. Nevertheless, resorting to a structure-guided drug design strategy, PLX5622 was created based on PLX3397, and has higher specificity for CSF1R than PLX3397 [32, 65, 66]. As previously reported, 7 days of PLX5622 treatment hardly affected OPC numbers in adult mice and 21 days of treatment only led to a mild OPC number reduction; in contrast, 7 days of PLX3397 treatment caused significant OPC loss [67]. As shown in Fig. S7, 10 days of PLX5622 treatment didn't result in significant variation of PDGFRα$^+$ OPC numbers in the somatosensory cortex, hippocampal CA1 and striatum areas of male *Cntnap2* KO. Therefore, we used PLX5622 in this study and persisted that

PLX5622 acts through inhibiting CSF1R signaling in microglia. However, we couldn't exclude a possibility that PLX5622 has side effects inside and outside the CNS, since PLX5622 was observed to affect "the turnover and function of bone marrow-derived, circulating, and tissue-resident macrophages" [68]. Whether such an effect on macrophages contributes to behavioral phenotype of the two autism model mice needs further investigation.

Fourthly, why were the two models of mice not subjected to the same battery of behavioral tests? That is, as reported in Figs. 1 and 5, marble burying test was not displayed in *Cntnap2* KO mice, while nest building test was not in VPA model mice. In line with the previous report by Penagarikano et al. [42], we did observe that *Cntnap2* KO mice were more focused on nestlet shredding and earned less scores in nest building test than WT (Fig. 2E). However, *Cntnap2* KO mice, whether or not treated by PLX5622, hardly buried marbles, whereas WT did (Fig. S8). Coincidentally, to the best of our knowledge, marble-burying test in *Cntnap2* KO mice has never been reported. In contrast, we observed that VPA model mice buried more marbles than the saline group (Fig. 6E), which is agreement with a dozen of previous reports [69–80]. Likely due to different genetic background in mice, different texture in nestlet and different testing environment employed, we didn't observe that VPA model mice shredded nestlet (data not shown) as previously reported by the same lab [73, 79, 81]. Both hyper- and hypo-responsiveness to tactile stimulation are recognized as diagnostic criteria for ASD [82], and mice have an innate preference for novel stimuli and can discriminate between the textures of the objects [83]. It is possible that *Cntnap2* KO and VPA model mice have different somatosensory preference for tactile stimuli invoked by marbles and nestlets. Therefore, nest-building and grooming tests were used to characterize the effects of PLX5622 on repetitive and stereotyped behaviors of *Cntnap2* KO mice (Fig. 2), and marble-burying and grooming tests were used for VPA model mice (Fig. 6).

Pharmacological effects of PLX5622 on Cntnap2 KO and VPA model mice

For the *Cntnap2* KO mice, PLX5622 can improve their sociability and reciprocal social behavior, slow down their hyperactivity and repetitive grooming behavior, and enhance their nesting ability. To investigate the role of microglia in *Cntnap2* KO behavior alteration, we checked microglial number and morphology. In this study, knockout of *Cntnap2* led to increased number and abnormal morphology of microglia in the cortical, hippocampal and striatum regions of male C57BL/6 J mice on P65. Different from our observation, Cope et al. found that the number or morphology of microglia in the hippocampus, medial prefrontal cortex and striatum in 5- to 6-month-old *Cntnap2* KO mice do not alter when compared with that in WT mice [24]. It seems that microglial abnormalities in *Cntnap2* KO mice can recover over time. Whether behavior deficits of *Cntnap2* KO mice may be alleviated at old ages needs further investigation. Nevertheless, when compared with WT, male *Cntnap2* KO mice have more activated microglia at P8 and P14 in the anterior cingulate cortex as observed by Dawson et al. [57] and at P21 in the somatosensory cortex and striatum areas as found in this study (Fig. S6). Therefore, we propose that microglial abnormalities at early in postnatal development may lead to autism-like behavioral deficits in male *Cntnap2* KO mice. Social cognition deficits in animal models of ASD have been linked to the cortex [84]. From this point of view, increased number and abnormal morphology of microglia in the cortical region of *Cntnap2* KO mice is likely a driver event causing weaken sociability, since PLX5622 can reset microglia in this region to the WT level and improve sociability deficits of *Cntnap2* KO mice. Meanwhile, it has been reported that striatal dysfunction is a neurological substrate for repetitive behaviors [2, 85]. From this perspective, microglial abnormality in the striatum of *Cntnap2* KO mice may lead to striatal dysfunction and therefore constitute pathological basis for repetitive behaviors, since repetitive grooming and nestlet-tearing behaviors of *Cntnap2* KO mice can be corrected by PLX5622-mediated microglial repopulation (Figs. 2, 3). As we know, microglia have an established role in modifying synapse and even can mediate changes of dendritic spine morphology [86, 87]. Dendritic spine morphology change was not observed in the cortical and hippocampal regions, but statistically significant in the striatum of the *Cntnap2* KO mice when compared with the WT counterparts (Fig. 4). It is reasonable that microglial abnormalities in the cortical and hippocampal regions might modify synapses, rather than dendritic spine morphology, to impair social behaviors of the *Cntnap2* KO mice. In comparison, microglial abnormalities in the striatum of the *Cntnap2* KO mice coalesce with dendritic spine subtype variation, and PLX5622 treatment resets microglia to a ramified state alongside re-distribution of dendritic spine subtype and improvement of repetitive behaviors (Figs. 2, 3, 4). CASPR2 is present in dendritic spines [88] and enriched in the synaptic plasma membrane to regulate the excitation/inhibition (E/I) balance [89]. Indeed, it has been reported that mouse offspring exposed to CASRP2-antibodies exhibit social interaction deficits, impaired nesting ability, persistent microglial activation and decreased glutamatergic synapses in the prefrontal and somatosensory cortices [23]. It is possible that microglia might affect dendritic spine morphology and mediate the E/I balance of local

circuitry for behavioral changes in *Cntnap2* KO using a way similar to that of prenatally CASPR2 antibodies-exposed mice.

For the VPA model mice, PLX5622 can significantly improve their social ability and social novelty, anxiety behavior, repetitive grooming and stereotyped marble-burying behaviors. As the most significant difference from the case of *Cntnap2* KO mice, PLX5622 effectively improve social novelty of the VPA model mice in the second phase of three chamber social interaction test, with distinctly increased sniffing time with Stranger 2. Unlike the case of the *Cntnap2* KO mice, microglial number and morphology, as well as dendritic spine density and subtype, significantly changed in the hippocampal CA1 region of the VPA model mice compared with the saline group. Conceivably, PLX5622-controlled microglia replacement and dendrite spine morphology recovery in hippocampal CA1 likely have influence on the CA2 region, a brain region essential for social memory [90], so that social novelty of the VPA model mice can be improved. In addition, we also observed dynamic changes of number or morphology of microglia in the VPA model mice, and suggested a dynamic process of microglia in autism animal model is similar to that of other neurological and psychiatric disorder models [27, 91]. Noteworthy, to the best of our knowledge, this study provides the first evidence of microglial dynamics in an autism model animal. As an environmental risk factor, prenatal VPA exposure leads to epigenetic processes that regulates gene expressions [43], and therefore likely influences neuronal development, dendritic spine morphology and microglia-neuron interaction in multiple brain regions. PLX5622 alleviates behavioral deficits in the VPA model mice likely through rescuing microglia-neuron crosstalk insulted by VPA epigenetic modification.

Potential mechanisms underlying microglia-mediated neuronal circuits and behavioral modification in Cntnap2 KO and VPA model mice

Overall, short-term suppression of CSF1R signaling by PLX5622 led to microglial depletion and repopulation, and improved social deficits, repetitive and other autism-like behaviors in the Cntnap2 KO and prenatal VPA-exposure autism model mice. As depicted above, the changes of microglia, neuronal dendritic spines in various brain regions and behavioral phenotypes are not exclusively identical in the two models. This reflects shared but differential potential mechanisms underlying how microglia may contribute to neuronal circuits and behavioral phenotypes in *Cntnap2* KO and VPA model mice.

As mentioned above, microglia in the rodent brain under normal physiological conditions present highly activated state during the postnatal three weeks, and microglia number reach the maximal level at P21 [51]. Meanwhile, glial cell-dependent synaptic pruning contributes to brain circuit refinement in two phases: the primary phase corresponding to the postnatal three weeks in mice, and the second phase that is referred to adolescence in mammals, for example, the postnatal 3–8 weeks in mice [92–94]. The primary phase of synaptic pruning ensures the proper formation of sensory and executive circuits responsible for processing tactile and other sensory information or for regulating memory, while the second phase of synaptic pruning pronouncedly occurs in brain regions that require remodeling for high functioning and goal planning [92, 95, 96]. It seems that P21 is a critical timeline for synaptic pruning and circuit formation in mouse. Therefore, we checked microglia number and morphology in *Cntnap2* KO and VPA model mice at P21 and selected this time point for microglia depletion. As shown in Fig. S6, Figs. 7 and 9, microglia in the somatosensory cortex and striatum areas of both *Cntnap2* KO and VPA model mice at P21 displayed more activated states than their normal counterparts. Correspondingly, lower dendritic spine density was observed in the somatosensory cortex and striatum of VPA model mice compared with the saline group (Fig. 10). Microglia activation and lower neuronal spine density in VPA model mice at P21 suggest that over synaptic pruning by microglia in the primary phase may result in improper circuits for tactile information processing. This may likely explain why both *Cntnap2* KO and VPA model mice exhibited impaired behaviors in nestlet shredding or marble burying (Figs. 2D and 6D). After 10 days of depletion by PLX5622, microglia in both *Cntnap2* KO and VPA underwent repopulation and gradually recovered to the normal level at P65 (Figs. 3 and 7, 8, 9). Correspondingly, neuronal spine density and mature spine numbers in the striatum of the two models also restored to the normal level (Figs. 4I–L and 10 I–L), and their ASD-like behaviors were partially or totally corrected (Figs. 1, 2, 5 and 6). These data implicate that repopulated microglia may push the second phase of synaptic pruning back to a correct track so that proper circuits coding for high functions, such as social interaction and nest building, are likely re-formed.

Noteworthy, no significant difference was observed for microglia number and morphology in the hippocampal CA1 area between male *Cntnap2* KO and WT at P21, whereas higher microglia density, more activated state of microglia and lower neuronal dendritic spine density were seen in this region of VPA model mice at this time point (Fig. 6S and Fig. 8). This suggests that microglia in VPA model mice may have more profound influence on neural circuit in the hippocampal CA1 than that in

Cntnap2 KO. Indeed, a recent study has demonstrated that prenatal VPA exposure invoked microglial activation and neural circuit dysfunction in the hippocampal CA1 region during the early postnatal periods [69]. In contrast, the striatum is the only tested area in *Cntnap2* KO at P65 to see synchronized recovery of microglia morphology and neuronal spine density to the WT level (Figs. 3, 4). Intriguingly, the ventral striatum network is an exception to see abnormal connectivity in *Cntnap2* KO at P58 [97]. This suggests that microglia may remodel neuronal circuit in the striatum of *Cntnap2* KO through directly regulating neuronal spine plasticity in the adolescent period.

As pointed out earlier, although no change of dendritic spine density was observed in the somatosensory and hippocampal CA1 regions of *Cntnap2* KO at P65, microglia in the two areas restored to the WT level upon PLX5622 treatment (Figs. 3 and 4). This implicates that microglia may remodel circuits in these areas through other functions, instead of direct synapse phagocytosis. Accumulating evidence shows that microglia can release growth factors and cytokines, such as TGFβ [9], BDNF [98] and Wnt5a [99], to regulate dendritic spine maintenance and alter neural circuitry. Moreover, upon activation by cytokine IL-33, microglia can engulf the extracellular matrix around synapses to promote synaptic plasticity [100]. Indeed, some cytokines, like BDNF [74] and Wnt5a [101], can signal to ERK1/2, a signal molecule on the MAPK pathway that can be upregulated by CSF1R signaling. Moreover, the MAPK cascade is one of signaling pathways related to microglial inflammatory response in VPA model mice [102]. Prenatal exposure to VPA can lead to epigenetic up-regulation of BDNF in VPA model mice[103]. Reasonably, CSF1R inhibition by PLX5622 might suppress improper cytokine-mediated circuits and downregulate microglia-mediated neuroinflammation in VPA model mice. Incidentally, there is no report about cytokine expression or inflammation in *Cntnap2* KO model except LPS-induced production of proinflammatory cytokine IL-17a [104]. Nevertheless, upregulation of another proinflammatory cytokine IL-6, which can suppress synapse pruning [105], was observed in the brain and cerebrospinal fluid of individuals with ASD [106], and blocking IL-6 receptor signaling can alleviate CASPR2 autoantibodies-associated syndrome [107], implicating that IL-6 might engage in inflammation or microglia function in *Cntnap2* KO. How cytokines change and mediate microglial function in remodeling synapses and circuits in *Cntnap2* KO and VPA model mice needs further investigation.

At the molecular level, VPA can promote epigenetic modification of a wide range of gene expressions in multiple brain regions [43]. In comparison, the expression profile of *Cntnap2* overlaps tightly with corticostriatothalamic circuitry [108], and CASPR2, a single-pass transmembrane neuronal adhesion molecule encoded by *Cntnap2*, exerts functions likely through engagement in protein–protein interaction [109]. Therefore, it is understandable that *Cntnap2* KO and VPA model mice might have differential mechanisms in remodeling circuits by microglia that reflects the heterogeneity of microglia. It is a limitation of this study that we didn't further probe microglia heterogeneity at the molecular level. In the future, it will be needed to use scRNA-seq technology to elucidate how microglial subsets are linked to behavioral variations in *Cntnap2* KO and VPA models.

In summary, *Cntnap2* KO and VPA model mice share commonality and difference in the timeline of microglia overactivation and depletion, the location of neuronal dendritic spine abnormalities, and the potential mechanism underlying circuit modification. Correspondingly, CSF1R inhibition by PLX5622 has pharmacological effectiveness and heterogeneity in correcting behavioral deficits of the two models. In line with our observation in this study, excessive microglia activation occurs in shared but different brain regions of some individuals with ASD [10, 11, 13], and microglia phenotypes present diversity [8, 15]. This implicates that CSF1R inhibition might be an effective strategy for clinical treatment of ASD, and that individual differences should also be considered.

Abbreviations

ASD	Autism spectrum disorder
CSF1R	Colony stimulating factor 1-receptor
FOV	Field of view
HPLC	High performance liquid chromatography
IVCs	Individually ventilated cages
KO	Knockout
LPS	Lipopolysaccharide
MIA	Maternal immune activation
NMR	Nuclear magnetic resonance spectroscopy
OCT	Optimal cutting temperature
PET	Positron emission tomography
PFA	Paraformaldehyde
poly I:C	Polyinosinic:polycytidylic acid
SEM	Standard error of the mean
VPA	Valproic acid
WT	Wildtype

Supplementary Information

The online version contains supplementary material available at https://doi.org/10.1186/s12974-024-03259-5.

Additional file1 (DOCX 31393 KB)

Acknowledgements

We thank Professor Jiada Li in Central South University for the gift of Cntnap2 heterozygous mice, and Professor Rong Zhang and Dr Xiaoxi Wang for helpful guidance in generating VPA model mice.

Author contributions

H.L. conceived the study. H.L. and J.M. designed experiments. J.M. performed experiments. X.M. and P.P. synthesized CSF1R inhibitor PLX5622. J.M., G.G. and

A.C. recorded behaviors of mice. J.M. and H.L. analyzed the data and wrote the manuscript. All authors reviewed the manuscript.

Funding
This work was supported by National Natural Science Foundation of China (grant No. 82173912) and the intramural research support program of 'Top Disciplines-Biomedicine' in Peking University Health Science Center (grant No. 73201Y1248).

Availability of data and materials
No datasets were generated or analysed during the current study.

Declarations

Ethics approval and consent to participate
All experimental procedures were in strict accordance with the recommendations in the Guide for the Care and Use of Laboratory Animals and approved by the institutional Animal Care and Use Committee on the Ethics of Animal Experiments of the Peking University Health Science Center (ethics approval ID, LA2021258).

Competing interests
The authors declare no competing interests.

Author details
[1]State Key Laboratory of Natural and Biomimetic Drugs, Peking University Health Science Center, 38 Xueyuan Road, Haidian District, Beijing 100191, China. [2]Department of Molecular and Cellular Pharmacology, School of Pharmaceutical Sciences, Peking University Health Science Center, 38 Xueyuan Road, Haidian District, Beijing 100191, China. [3]Department of Chemical Biology, School of Pharmaceutical Sciences, Peking University Health Science Center, 38 Xueyuan Road, Haidian District, Beijing 100191, China. [4]Autism Research Center, Peking University Health Science Center, 38 Xueyuan Road, Haidian District, Beijing 100191, China.

Received: 6 January 2024 Accepted: 8 October 2024
Published online: 18 October 2024

References

1. Spooren W, et al. Synapse dysfunction in autism: a molecular medicine approach to drug discovery in neurodevelopmental disorders. Trends Pharmacol Sci. 2012;33(12):669–84.
2. Jiang CC, et al. Signalling pathways in autism spectrum disorder: mechanisms and therapeutic implications. Signal Transduct Target Ther. 2022;7(1):229.
3. Fombonne E, MacFarlane H, Salem AC. Epidemiological surveys of ASD: advances and remaining challenges. J Autism Dev Disord. 2021;51(12):4271–90.
4. Estes ML, McAllister AK. Immune mediators in the brain and peripheral tissues in autism spectrum disorder. Nat Rev Neurosci. 2015;16(8):469–86.
5. Kreutzberg GW. Microglia: a sensor for pathological events in the CNS. Trends Neurosci. 1996;19(8):312–8.
6. Tay TL, et al. Microglia across the lifespan: from origin to function in brain development, plasticity and cognition. J Physiol. 2017;595(6):1929–45.
7. Tremblay ME, et al. The role of microglia in the healthy brain. J Neurosci. 2011;31(45):16064–9.
8. Morgan JT, et al. Microglial activation and increased microglial density observed in the dorsolateral prefrontal cortex in autism. Biol Psychiatry. 2010;68(4):368–76.
9. Vargas DL, et al. Neuroglial activation and neuroinflammation in the brain of patients with autism. Ann Neurol. 2005;57(1):67–81.
10. Tetreault NA, et al. Microglia in the cerebral cortex in autism. J Autism Dev Disord. 2012;42(12):2569–84.
11. Suzuki K, et al. Microglial activation in young adults with autism spectrum disorder. JAMA Psychiat. 2013;70(1):49–58.
12. Edmonson C, Ziats MN, Rennert OM. Altered glial marker expression in autistic post-mortem prefrontal cortex and cerebellum. Mol Autism. 2014;5(1):3.
13. Gupta S, et al. Transcriptome analysis reveals dysregulation of innate immune response genes and neuronal activity-dependent genes in autism. Nat Commun. 2014;5:5748.
14. Corbett BA, et al. A proteomic study of serum from children with autism showing differential expression of apolipoproteins and complement proteins. Mol Psychiatry. 2007;12(3):292–306.
15. Lee AS, Azmitia EC, Whitaker-Azmitia PM. Developmental microglial priming in postmortem autism spectrum disorder temporal cortex. Brain Behav Immun. 2017;62:193–202.
16. Morgan JT, et al. Stereological study of amygdala glial populations in adolescents and adults with autism spectrum disorder. PLoS ONE. 2014;9(10): e110356.
17. Bronzuoli MR, et al. Neuroglia in the autistic brain: evidence from a preclinical model. Mol Autism. 2018;9:66.
18. Sanagi T, et al. Segmented Iba1-positive processes of microglia in Autism model marmosets. Front Cell Neurosci. 2019;13:344.
19. Li X, et al. Microglia activation in the offspring of prenatal Poly I: C exposed rats: a PET imaging and immunohistochemistry study. Gen Psychiatr. 2018;31(1): e000006.
20. Malkova NV, et al. Maternal immune activation yields offspring displaying mouse versions of the three core symptoms of autism. Brain Behav Immun. 2012;26(4):607–16.
21. Jawaid S, et al. Alterations in CA1 hippocampal synapses in a mouse model of fragile X syndrome. Glia. 2018;66(4):789–800.
22. Heo Y, et al. Aberrant immune responses in a mouse with behavioral disorders. PLoS ONE. 2011;6(7): e20912.
23. Coutinho E, et al. Persistent microglial activation and synaptic loss with behavioral abnormalities in mouse offspring exposed to CASPR2-antibodies in utero. Acta Neuropathol. 2017;134(4):567–83.
24. Cope EC, et al. Immature neurons and radial glia, but not astrocytes or microglia, are altered in adult Cntnap2 and Shank3 mice models of Autism. eNeuro. 2016. https://doi.org/10.1523/ENEURO.0196-16.2016.
25. Prinz M, Jung S, Priller J. Microglia biology: one century of evolving concepts. Cell. 2019;179(2):292–311.
26. Andoh M, Ikegaya Y, Koyama R. Microglia as possible therapeutic targets for autism spectrum disorders. Prog Mol Biol Transl Sci. 2019;167:223–45.
27. Elmore MR, et al. Colony-stimulating factor 1 receptor signaling is necessary for microglia viability, unmasking a microglia progenitor cell in the adult brain. Neuron. 2014;82(2):380–97.
28. Han J, et al. Inhibition of colony stimulating factor-1 receptor (CSF-1R) as a potential therapeutic strategy for neurodegenerative diseases: opportunities and challenges. Cell Mol Life Sci. 2022;79(4):219.
29. Basilico B, et al. What microglia depletion approaches tell us about the role of microglia on synaptic function and behavior. Front Cell Neurosci. 2022;16:1022431.
30. Yamamoto M, et al. Microglia-triggered plasticity of intrinsic excitability modulates psychomotor behaviors in acute cerebellar inflammation. Cell Rep. 2019;28(11):2923-2938 e8.
31. Dwyer Z, et al. Microglia depletion prior to lipopolysaccharide and paraquat treatment differentially modulates behavioral and neuronal outcomes in wild type and G2019S LRRK2 knock-in mice. Brain Behav Immun Health. 2020;5: 100079.
32. Spangenberg E, et al. Sustained microglial depletion with CSF1R inhibitor impairs parenchymal plaque development in an Alzheimer's disease model. Nat Commun. 2019;10(1):3758.
33. Olmos-Alonso A, et al. Pharmacological targeting of CSF1R inhibits microglial proliferation and prevents the progression of Alzheimer's-like pathology. Brain. 2016;139(Pt 3):891–907.
34. Henry RJ, et al. Microglial depletion with CSF1R inhibitor during chronic phase of experimental traumatic brain injury reduces neurodegeneration and neurological deficits. J Neurosci. 2020;40(14):2960–74.
35. Willis EF, et al. Repopulating microglia promote brain repair in an IL-6-dependent manner. Cell. 2020;180(5):833-846 e16.
36. Tahmasebi F, et al. Effect of the CSF1R inhibitor PLX3397 on remyelination of corpus callosum in a cuprizone-induced demyelination mouse model. J Cell Biochem. 2019;120(6):10576–86.

37. Crapser JD, et al. Microglial depletion prevents extracellular matrix changes and striatal volume reduction in a model of Huntington's disease. Brain. 2020;143(1):266–88.
38. Ikezu S, et al. Inhibition of colony stimulating factor 1 receptor corrects maternal inflammation-induced microglial and synaptic dysfunction and behavioral abnormalities. Mol Psychiatry. 2021;26(6):1808–31.
39. Torres L, et al. Dynamic microglial modulation of spatial learning and social behavior. Brain Behav Immun. 2016;55:6–16.
40. Kreisel T, et al. Dynamic microglial alterations underlie stress-induced depressive-like behavior and suppressed neurogenesis. Mol Psychiatry. 2014;19(6):699–709.
41. Hohsfield LA, et al. Subventricular zone/white matter microglia reconstitute the empty adult microglial niche in a dynamic wave. Elife. 2021. https://doi.org/10.7554/eLife.66738.
42. Penagarikano O, et al. Absence of CNTNAP2 leads to epilepsy, neuronal migration abnormalities, and core autism-related deficits. Cell. 2011;147(1):235–46.
43. Nicolini C, Fahnestock M. The valproic acid-induced rodent model of autism. Exp Neurol. 2018;299(Pt A):217–27.
44. Xing X, et al. Suppression of Akt-mTOR pathway rescued the social behavior in Cntnap2-deficient mice. Sci Rep. 2019;9(1):3041.
45. Deacon RM. Assessing nest building in mice. Nat Protoc. 2006;1(3):1117–9.
46. Buffington SA, et al. Dissecting the contribution of host genetics and the microbiome in complex behaviors. Cell. 2021;184(7):1740-1756 e16.
47. Silverman JL, et al. Sociability and motor functions in Shank1 mutant mice. Brain Res. 2011;1380:120–37.
48. Szczypka MS, et al. Dopamine production in the caudate putamen restores feeding in dopamine-deficient mice. Neuron. 2001;30(3):819–28.
49. Han J, et al. Enforced microglial depletion and repopulation as a promising strategy for the treatment of neurological disorders. Glia. 2019;67(2):217–31.
50. Ferri SL, Abel T, Brodkin ES. Sex differences in Autism spectrum disorder: a review. Curr Psychiatry Rep. 2018;20(2):9.
51. Schwarz JM, Sholar PW, Bilbo SD. Sex differences in microglial colonization of the developing rat brain. J Neurochem. 2012;120(6):948–63.
52. Guneykaya D, et al. Transcriptional and translational differences of microglia from male and female brains. Cell Rep. 2018;24(10):2773-2783 e6.
53. Hammond TR, et al. Single-Cell RNA sequencing of microglia throughout the mouse lifespan and in the injured brain reveals complex cell-state changes. Immunity. 2019;50(1):253-271 e6.
54. VanRyzin JW, et al. Microglial phagocytosis of newborn cells is induced by endocannabinoids and sculpts sex differences in juvenile rat social play. Neuron. 2019;102(2):435-449 e6.
55. McCarthy MM, Nugent BM, Lenz KM. Neuroimmunology and neuroepigenetics in the establishment of sex differences in the brain. Nat Rev Neurosci. 2017;18(8):471–84.
56. Schaafsma SM, et al. Sex-specific gene-environment interactions underlying ASD-like behaviors. Proc Natl Acad Sci U S A. 2017;114(6):1383–8.
57. Dawson MS, et al. Sexual dimorphism in the social behaviour of Cntnap2-null mice correlates with disrupted synaptic connectivity and increased microglial activity in the anterior cingulate cortex. Commun Biol. 2023;6(1):846.
58. Mowery TM, et al. Embryological exposure to valproic acid disrupts morphology of the deep cerebellar nuclei in a sexually dimorphic way. Int J Dev Neurosci. 2015;40:15–23.
59. Kim KC, et al. Male-specific alteration in excitatory post-synaptic development and social interaction in pre-natal valproic acid exposure model of autism spectrum disorder. J Neurochem. 2013;124(6):832–43.
60. Kazlauskas N, et al. Sex-specific effects of prenatal valproic acid exposure on sociability and neuroinflammation: relevance for susceptibility and resilience in autism. Psychoneuroendocrinology. 2019;110: 104441.
61. Lenz KM, Nelson LH. Microglia and beyond: innate immune cells as regulators of brain development and behavioral function. Front Immunol. 2018;9:698.
62. Paolicelli RC, et al. Microglia states and nomenclature: a field at its crossroads. Neuron. 2022;110(21):3458–83.
63. Lemmon MA, Schlessinger J. Cell signaling by receptor tyrosine kinases. Cell. 2010;141(7):1117–34.
64. Nishiyama A, et al. Polydendrocytes (NG2 cells): multifunctional cells with lineage plasticity. Nat Rev Neurosci. 2009;10(1):9–22.
65. Dagher NN, et al. Colony-stimulating factor 1 receptor inhibition prevents microglial plaque association and improves cognition in 3xTg-AD mice. J Neuroinflammation. 2015;12:139.
66. Kim TS, et al. Increased KIT inhibition enhances therapeutic efficacy in gastrointestinal stromal tumor. Clin Cancer Res. 2014;20(9):2350–62.
67. Liu Y, et al. Concentration-dependent effects of CSF1R inhibitors on oligodendrocyte progenitor cells ex vivo and in vivo. Exp Neurol. 2019;318:32–41.
68. Lei F, et al. CSF1R inhibition by a small-molecule inhibitor is not microglia specific; affecting hematopoiesis and the function of macrophages. Proc Natl Acad Sci U S A. 2020;117(38):23336–8.
69. Ishihara Y, et al. A CCR5 antagonist, maraviroc, alleviates neural circuit dysfunction and behavioral disorders induced by prenatal valproate exposure. J Neuroinflammation. 2022;19(1):195.
70. Reza Naghdi M, et al. The neuroprotective effect of Diosgenin in the rat Valproic acid model of autism. Brain Res. 2024;1838: 148963.
71. Mehta MV, Gandal MJ, Siegel SJ. mGluR5-antagonist mediated reversal of elevated stereotyped, repetitive behaviors in the VPA model of autism. PLoS ONE. 2011;6(10): e26077.
72. Liu Z, et al. Vitamin A supplementation ameliorates prenatal valproic acid-induced autism-like behaviors in rats. Neurotoxicology. 2022;91:155–65.
73. Eissa N, et al. The histamine H3R antagonist DL77 attenuates autistic behaviors in a prenatal valproic acid-induced mouse model of autism. Sci Rep. 2018;8(1):13077.
74. Chen S, et al. The prenatal use of agmatine prevents social behavior deficits in VPA-exposed mice by activating the ERK/CREB/BDNF signaling pathway. Birth Defects Res. 2024;116(4): e2336.
75. Wang K, et al. Glyoxalase 1 inhibitor alleviates Autism-like phenotype in a prenatal valproic acid-induced mouse model. ACS Chem Neurosci. 2020;11(22):3786–92.
76. Taheri F, et al. Amelioration of cognition impairments in the valproic acid-induced animal model of autism by ciproxifan, a histamine H3-receptor antagonist. Behav Pharmacol. 2023;34(4):179–96.
77. Soltani Z, et al. Investigating the effect of exposure to monosodium glutamate during pregnancy on development of autism in male rat offspring. Food Chem Toxicol. 2024;185: 114464.
78. Huang F, et al. Betaine ameliorates prenatal valproic-acid-induced Autism-like behavioral abnormalities in mice by promoting homocysteine metabolism. Psychiatry Clin Neurosci. 2019;73(6):317–22.
79. Eissa N, et al. The dual-active histamine H(3) receptor antagonist and acetylcholine esterase inhibitor E100 alleviates autistic-like behaviors and oxidative stress in valproic acid induced Autism in mice. Int J Mol Sci. 2020;21(11):3996.
80. Baronio D, et al. Effects of an H3R antagonist on the animal model of autism induced by prenatal exposure to valproic acid. PLoS ONE. 2015;10(1): e0116363.
81. Nakhal MM, et al. Canagliflozin ameliorates oxidative stress and autistic-like features in valproic-acid-induced autism in rats: comparison with aripiprazole action. Pharmaceuticals (Basel). 2023;16(5):769.
82. Association AP. Desk reference to the diagnostic criteria from DSM-5. Washington, DC: American Psychiatric Publishing; 2013.
83. Balasco L, et al. Somatosensory cortex hyperconnectivity and impaired whisker-dependent responses in Cntnap2(-/-) mice. Neurobiol Dis. 2022;169: 105742.
84. Bicks LK, et al. Prefrontal cortex and social cognition in mouse and man. Front Psychol. 2015;6:1805.
85. Langen M, et al. The neurobiology of repetitive behavior: …and men. Neurosci Biobehav Rev. 2011;35(3):356–65.
86. Miyamoto A, et al. Microglia contact induces synapse formation in developing somatosensory cortex. Nat Commun. 2016;7:12540.
87. Weinhard L, et al. Microglia remodel synapses by presynaptic trogocytosis and spine head filopodia induction. Nat Commun. 2018;9(1):1228.
88. Varea O, et al. Synaptic abnormalities and cytoplasmic glutamate receptor aggregates in contactin associated protein-like 2/Caspr2 knockout neurons. Proc Natl Acad Sci U S A. 2015;112(19):6176–81.
89. Bakkaloglu B, et al. Molecular cytogenetic analysis and resequencing of contactin associated protein-like 2 in autism spectrum disorders. Am J Hum Genet. 2008;82(1):165–73.

90. Banker SM, et al. Hippocampal contributions to social and cognitive deficits in autism spectrum disorder. Trends Neurosci. 2021;44(10):793–807.
91. Rice RA, et al. Microglial repopulation resolves inflammation and promotes brain recovery after injury. Glia. 2017;65(6):931–44.
92. Neniskyte U, Gross CT. Errant gardeners: glial-cell-dependent synaptic pruning and neurodevelopmental disorders. Nat Rev Neurosci. 2017;18(11):658–70.
93. Schafer DP, Stevens B. Microglia function in central nervous system development and plasticity. Cold Spring Harb Perspect Biol. 2015;7(10): a020545.
94. Sekar A, et al. Schizophrenia risk from complex variation of complement component 4. Nature. 2016;530(7589):177–83.
95. Johnson MH. Functional brain development in humans. Nat Rev Neurosci. 2001;2(7):475–83.
96. Blakemore SJ. Development of the social brain during adolescence. Q J Exp Psychol (Hove). 2008;61(1):40–9.
97. Zerbi V, et al. Dysfunctional Autism risk genes cause circuit-specific connectivity deficits with distinct developmental trajectories. Cereb Cortex. 2018;28(7):2495–506.
98. Komori T, et al. Brain-derived neurotrophic factor from microglia regulates neuronal development in the medial prefrontal cortex and its associated social behavior. Mol Psychiatry. 2024;29(5):1338–49.
99. Yeh H, et al. Microglial WNT5A supports dendritic spines maturation and neuronal firing. Brain Behav Immun. 2023;107:403–13.
100. Nguyen PT, et al. Microglial remodeling of the extracellular matrix promotes synapse plasticity. Cell. 2020;182(2):388-403 e15.
101. Halleskog C, et al. Heterotrimeric G protein-dependent WNT-5A signaling to ERK1/2 mediates distinct aspects of microglia proinflammatory transformation. J Neuroinflammation. 2012;9:111.
102. Zhang Q, et al. Sex-biased single-cell genetic landscape in mice with autism spectrum disorder. J Genet Genom. 2024;51(3):338–51.
103. Konopko MA, Densmore AL, Krueger BK. Sexually dimorphic epigenetic regulation of brain-derived neurotrophic factor in fetal brain in the valproic acid model of Autism spectrum disorder. Dev Neurosci. 2017;39(6):507–18.
104. Reed MD, et al. IL-17a promotes sociability in mouse models of neurodevelopmental disorders. Nature. 2020;577(7789):249–53.
105. Han VX, et al. Maternal immune activation and neuroinflammation in human neurodevelopmental disorders. Nat Rev Neurol. 2021;17(9):564–79.
106. Xu N, Li X, Zhong Y. Inflammatory cytokines: potential biomarkers of immunologic dysfunction in autism spectrum disorders. Mediat Inflamm. 2015;2015: 531518.
107. Krogias C, et al. Successful treatment of anti-Caspr2 syndrome by interleukin 6 receptor blockade through tocilizumab. JAMA Neurol. 2013;70(8):1056–9.
108. Abrahams BS, et al. Genome-wide analyses of human perisylvian cerebral cortical patterning. Proc Natl Acad Sci U S A. 2007;104(45):17849–54.
109. Liang W, et al. Structural mapping of hot spots within human CASPR2 discoidin domain for autoantibody recognition. J Autoimmun. 2019;96:168–77.

Publisher's Note